Aalto University
School of Chemical
Technology

School of Chemical Technology
Degree Programme of Material Science & Engineering

Matteo Vettorel

TITANIUM ALLOYS AND POROUS COATINGS FOR ORTHOPAEDIC APPLICATIONS

Final Project (30 cr) submitted for inspection, Espoo, 9th June 2014.

Supervisor **Professor Michael Gasik**

Instructor **Ph.D. Yevgen Bilotsky**

Aalto University
School of Chemical
Technology

Aalto University, P.O. BOX 11000, 00076 AALTO
www.aalto.fi

Abstract of Final Project

Author Matteo Vettorel

Title of final project TITANIUM ALLOYS AND POROUS COATINGS FOR ORTHOPAEDIC APPLICATIONS

Department Material Science and Engineering

Professorship Material Processing **Code of professorship** MT-77

Thesis supervisor Professor Michael Gasik

Thesis advisor(s) / Thesis examiner(s) Ph.D. Yevgen Bilotsky

Date 09.06.2014 **Number of pages** 82 **Language** English

Abstract

The project deals with titanium and titanium alloys as biomaterials for implants applications, focusing on their mechanical response under dynamic stresses occurring during common human activities. In the first part, the biomaterials requirements for orthopaedic implants, the properties and the processing of titanium alloys are described. From the combined biomechanics requirements, mechanical behaviour of the materials and the bone is analysed and the additional poroelastic behaviour is added for fluidic transport inside porous material undergoing oscillatory mechanical deformation. Based on these analyses, the biomechanical behaviour of titanium alloy for orthopaedic prosthesis is simulated by finite elements analysis with the software COMSOL Multiphysics. The simulations concern dynamic mechanical three-point bending coated specimens, studying the influence of porous coatings with different characteristics of thickness and porosity. Experimental tests with dynamic mechanical analysis (DMA) are performed in order to validate the model.

Keywords: Titanium Alloys, Orthopaedic Prosthesis, Mechanical Behaviour, Dynamic Mechanical Analysis, Porous Coating.

ACKNOWLEDGEMENT

This Final Project was carried out in Otaniemi, Espoo, at the Material Science and Engineering Department of Aalto University, during the period January – June 2014. This work represents the last step in my Materials Engineering Master Degree program at University of Padua, Italy. This Erasmus experience was certainly the most challenging and enriching in my life, giving me the opportunity to discover Finland and to meet new friends, whose memory will be always part of me.

I would like to express my thankfulness to professor Michael Gasik, my supervisor, who allowed me to perform this project, and to professor Franco Bonollo, who accommodate my request to be part of the Erasmus program.

I would like to express my gratitude and my all the people who made me feel like part of a family, spending time together and sharing our happiness each other: Nicolò, Stefano, Sellene, Raquel, Miquel and Gerard, I won't never forget our friendship.

Finally, but not least, I would like to express my deepest love to my parents, my brother Nicolò and my girlfriend Alessia, for their constant support and patience. They always encouraged me to do the best in all situations of my life and who I am I owe to them. This work is dedicated to all of you.

Espoo, 9TH June 2014

Matteo Vettorel

TABLE OF CONTENTS

LIST OF FIGURES

LIST OF TABLES

LIST OF SYMBOLS

A	area	[m^2]
C_{ij}	coefficients of the stiffness matrix	[Pa]
k	permeability	[m^2]
d	equivalent diameter	[m]
E	Young's modulus	[Pa]
E^*	time dependent Young's modulus	[Pa]
E'	storage modulus	[Pa]
E''	loss modulus	[Pa]
E_0	Young's modulus of non-porous bulk material	[Pa]
E_p	Young's modulus of porous material	[Pa]
F	force	[N]
g	magnitude of gravitational acceleration	[$m \cdot s^{-2}$]
G	shear modulus	[Pa]
i	imaginary unity	-
K	stress intensity factor	[$Pa \cdot m^{0.5}$]
K_{IC}	fracture toughness mode I	[$Pa \cdot m^{0.5}$]
K_{eff}	effective bulk modulus	[Pa]
K_f	fluid bulk modulus	[Pa]
K_s	solid bulk modulus	[Pa]
L	length	[m]
p	fluid pressure	[Pa]
p_p	pore pressure	[Pa]
R	stress ratio	-
Re	Reynolds number	-
u_D	fluid velocity (Darcy's flow)	[$m \cdot s^{-1}$]
u	Darcy velocity	[$m \cdot s^{-1}$]
U	fluid flow rate	[$m^3 \cdot s^{-1}$]
V_f	fluid volume	[m^3]
V_p	pore volume	[m^3]
V_s	solid matrix volume	[m^3]
V_t	total volume	[m^3]

GREEK LETTERS

α	Biot's coefficient	-
γ	shear strain	-
δ	phase angle	-
ε	strain	-
ζ	fluid content	-
θ_s	fluid volume fraction	-
μ	fluid's dynamic viscosity	[Pa·s]
ν	Poisson's ratio	-
ρ	density	[kg·m^{-3}]
ρ_0	density of non-porous bulk material	[kg·m^{-3}]
ρ_p	density of porous material	[kg·m^{-3}]
σ_f	fatigue strength	[Pa]
σ_R	bending-rotating fatigue strength	[Pa]
σ_y	yield stress	[Pa]
σ	normal stress	[Pa]
τ	shear stress	[Pa]
ϕ	porosity	-

LIST OF ABBREVIATIONS

ASTM	American Society for Testing and Materials
BCC	body centered cubic
CMP	COMSOL Multiphysics
CP	commercially pure
CVD	chemical vapour deposition
DMA	dynamic mechanical analysis
FE	finite element
FEA	finite element analysis
FFC	Fray – Farthing – Chen
GUI	graphical user interface
HAP	hydroxyapatite
HCP	hexagonal close packed
MRI	magnetic resonance imaging
NSEs	Navier-Stokes equations
PDEs	partial differential equations
PPM	parts per million
PVD	physical vapour deposition
SME	shape memory effect
SS	stainless steel
THR	total hip replacement
UTS	ultimate tensile strength
YS	yield strength
VAR	vacuum arc remelting

1 THE OBJECTIVES AND THE STRUCTURE OF THE WORK

The most important feature of biomaterials and implants is the improvement of human health and life quality. First attempts to use common material to favour healing date back to more than thousands years B.C., but rigorous scientific research on materials able to be tolerated in a living body started only during 19^{TH} century and it found first human successful applications in early decades of 20^{TH} century [1]. Technological improvements are currently made day by day through research in each of the fields involved in biomaterials, such as medicine, surgery, biology, chemistry and engineering. The common good of this multidisciplinary collaboration is the achievement of the best performance for an implant device, and the focus point in biomaterials research lies in the physical and chemical interactions between a complex biological system and artificial materials.

The engineering side of the biomaterial challenges concerns medical devices with the appropriate design, fabricated from the most suitable materials, to meet needs patients.

Both the biomaterial and the device affect the patient's host tissue, which itself affects the device: this interaction can lead to implant success or failure.

This work focuses on biomaterials for mainly orthopaedic applications (hip, knee, shoulder arthoplasties and some types of spinal instrumentation), and the main type of biomaterial described there is titanium alloy.

Main objectives of this study are the following:

- to analyse basic requirements for orthopaedic implants, especially for titanium alloys, their processing and application for implants
- to develop a mathematical model capable of simulation of the behaviour of Ti-alloy (porous coated or non-coated) samples subjected to three-point bending dynamic tests with oscillating force at a frequency compatible with human common activities
- to analyse the effect of specimens geometry and properties on their mechanical behaviour and

- to perform experimental tests to validate the model

This final project is organized as follows:

- The literature (theoretical) part involves four chapters. Chapter 2 presents fundamentals of linear elasticity theory, poroelasticity theory and porous flow governing equations, relevant for understanding of the application and necessary parameters for a successful materials solution. An introduction on biomaterials and their classification is given in chapter 3 , summarizing advantages or drawbacks of each class of biomaterials. Basic concepts on bone structure and bone properties are explained in chapter 4 , so as to introduce challenges and problems which engineers involved in bone replacement field have to deal with. Chapter 5 examines metallic biomaterials, primarily focusing on titanium as biomaterial, from its production to its application, emphasizing properties that make titanium alloys the most widespread materials in orthopaedics.
- Experimental part consists of three chapters: chapter 6 presents the dynamic mechanical simulations performed with the software Comsol MultiPhysics, while in chapter 7 results from laboratory experiments are showed and discussed.
- Final conclusions are presented in chapter 8 , complemented with cited references.

2 FUNDAMENTALS OF ELASTICITY, DYNAMIC MECHANICAL ANALYSIS AND POROELASTICITY

2.1 Elasticity

Elasticity is the ability of most of the materials to recover a part of the deformation produced by acting forces, and elasticity theory is based on the concepts of stress and strain. Stress is defined as the ratio of the acting force to the cross-section on which it is acting (Figure 1):

$$\sigma = \frac{F}{A} \tag{2.1}$$

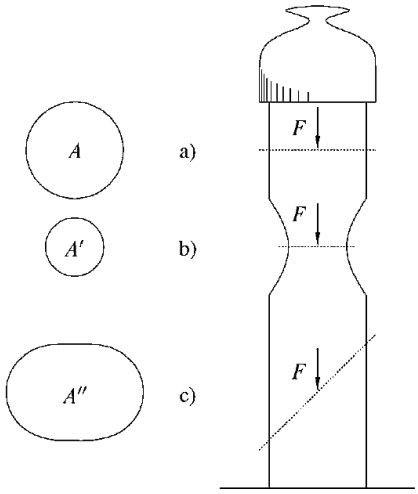

Figure 1: Concept of stress [2].

The SI unit for stress is the pascal [Pa], equivalent to [N·m^{-1}].

The strain is induced when, after the action of an external force on a representative portion of the material, the positions of two points O and P (Figure 2) cannot be described by a simply rigid translation and/or rotation of the sample. The quantity defined as

$$\varepsilon = \frac{L' - L}{L} = \frac{\Delta L}{L} \tag{2.2}$$

represents the elongation (if positive) or the contraction (if negative) occurring along the direction OP (Figure 2).

On the other hand, the quantity defined as

$$\gamma = \frac{1}{2}\tan\alpha \tag{2.3}$$

is the shear strain corresponding to the point O and the direction OP (Figure 3).

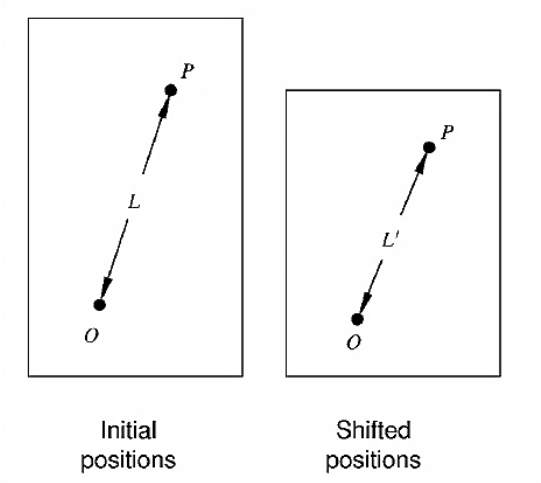

Figure 2: Deformation: contraction [2].

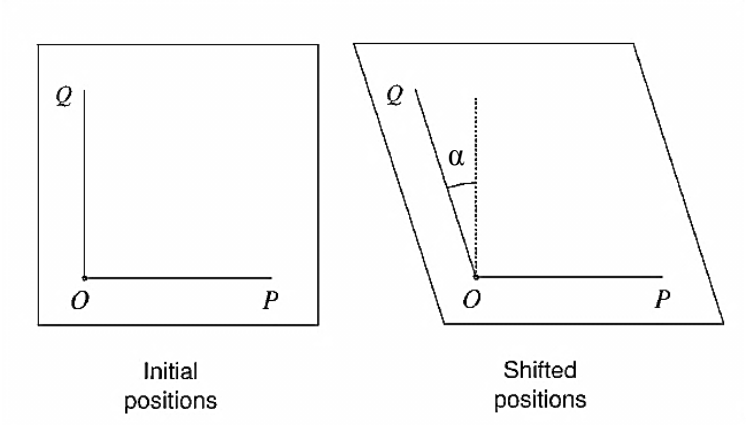

Figure 3: Shear deformation [2].

Common materials exhibit elastic behaviour, returning to their original configuration when the load is removed, only if the applied load is sufficiently small.

The theory of linear elasticity deals with situations where linear relations between applied stresses and consequent strains are recognized, and this behaviour is usually

valid for small stresses, causing infinitesimal strains. In this case, a linear relation between local stress and strain, the so called Hooke's law, is easily identified:

$$\sigma_{ij} = C_{ij}\varepsilon_{ij} \tag{2.4}$$

Where strain components ε_{ij} are derived from displacement derivatives:

$$\varepsilon_{ij} = \frac{1}{2}\left(\frac{\partial u_i}{\partial x_j} + \frac{\partial u_j}{\partial x_i}\right) \tag{2.5}$$

The subscripts i and j are indices that may take on any of the three values 1, 2 or 3, representing the x-, y- and z-axis, respectively.

The law gives a complete description of the stress state at a point P of an hypothetic representative element of the material: stresses generated by forces perpendicular to the cross-section are the normal stresses (usually written as σ), while those generated by forces parallel to the cross-section are shear stresses (τ). Considering the three orthogonal directions, all the nine possible stresses related to the point are described by the stress tensor:

$$\sigma = \begin{pmatrix} \sigma_{xx} & \tau_{xy} & \tau_{xz} \\ \tau_{yx} & \sigma_{yy} & \tau_{yz} \\ \tau_{zx} & \tau_{zy} & \sigma_{zz} \end{pmatrix} \tag{2.6}$$

To give a full description of the strain state at a point within a three-dimensional body, the elongation and shear strains corresponding to all three axes must be specified, and all strains are defined by (2.5), leading to the strain tensor:

$$\varepsilon = \begin{pmatrix} \varepsilon_{xx} & \varepsilon_{xy} & \varepsilon_{xz} \\ \varepsilon_{yx} & \varepsilon y_y & \varepsilon_{yz} \\ \varepsilon_{zx} & \varepsilon_{zy} & \varepsilon_{zz} \end{pmatrix} \tag{2.7}$$

The coefficient of the 6×6 stiffness matrix $[C_{ij}]$ in (2.4) linking σ and ε are generally not constant, but energy assumptions show that it is symmetric, reducing the number of independent elastic constants from 36 to 21 for a complete anisotropic material [3]. The number of independent elastic constants can be further decreased assuming that the material has some type of symmetry (Figure 4).

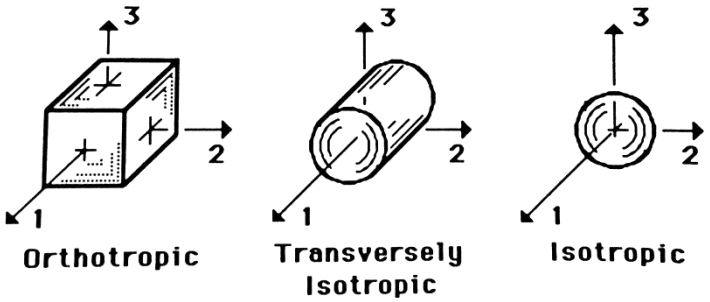

Figure 4: Graphical representations of three material symmetries [3].

Orthotropic symmetry (three mutually perpendicular planes of symmetry) requires that nine of the twelve non-zero coefficients appearing in the matrix $[C_{ij}]$ have to be independent:

$$[C_{ij}] = \begin{bmatrix} C_{11} & C_{12} & C_{13} & 0 & 0 & 0 \\ C_{12} & C_{22} & C_{23} & 0 & 0 & 0 \\ C_{13} & C_{23} & C_{33} & 0 & 0 & 0 \\ 0 & 0 & 0 & C_{44} & 0 & 0 \\ 0 & 0 & 0 & 0 & C_{55} & 0 \\ 0 & 0 & 0 & 0 & 0 & C_{66} \end{bmatrix} \tag{2.8}$$

Furthermore, transversely isotropic materials have an axis of symmetry in addition to three planes of symmetry: in the stiffness matrix will appear five independent elastic constants C_{ij} and twelve non-zero terms:

$$[C_{ij}] = \begin{bmatrix} C_{11} & C_{12} & C_{13} & 0 & 0 & 0 \\ C_{12} & C_{11} & C_{13} & 0 & 0 & 0 \\ C_{13} & C_{13} & C_{33} & 0 & 0 & 0 \\ 0 & 0 & 0 & C_{44} & 0 & 0 \\ 0 & 0 & 0 & 0 & C_{44} & 0 \\ 0 & 0 & 0 & 0 & 0 & C_{66} \end{bmatrix} \tag{2.9}$$

Where $C_{66} = \frac{1}{2}(C_{11} - C_{12})$.

More simplification is possible with isotropic materials: they have only two independent constants in the stiffness matrix, because the response of the material is not dependent of the stress direction.

Factors of proportionality that describe elastic responses of a material to applied forces are the so-called elastic constants (or elastic moduli). In case of linear elastic behaviour, the relation

$$\varepsilon_x = \frac{1}{E}\sigma_x \tag{2.10}$$

introduces the coefficient E, called Young's modulus or simply elastic modulus. It measures the tendency of the material to deform along an axis when tensile (or compressive) forces are applied along that axis: it is experimentally determined from the initial slope of the stress–strain curve created during tensile tests on standard material specimens.

Another elastic parameter, the Poisson's ratio ν, which measures the lateral contraction relative to longitudinal expansion, is defined as:

$$\nu = -\frac{\varepsilon_y}{\varepsilon_x} \tag{2.11}$$

As a tensile load applied along the x-axis usually provokes striction along the y/z-axis, Poisson's ratio is a positive dimensionless number; but materials exist with a negative value of ν (i.e. cork, particular foam structures…): it is bounded by two theoretical limits and its value must lie in the range $-1 < \nu < 0.5$.

Another elastic modulus, the shear modulus G, which measure the material's resistance against shear deformation, is defined as the ratio of shear stress to the shear strain:

$$G = -\frac{\tau_{xy}}{\gamma_{xy}} \tag{2.12}$$

Finally, the bulk modulus K is the ratio of the hydrostatic stress relative to the volumetric strain, defined as:

$$K = \frac{\sigma_p}{\varepsilon_{vol}} \tag{2.13}$$

In case of isotropic material, only two of these four moduli are independent, and simply relations may be derived. On the other hand, for anisotropic materials, elastic

properties change along different directions, except for the bulk modulus, which is invariant.

Ideally, elastic materials give a linear response regardless load and loading rate values, but for real materials the elastic behaviour is maintained until the elastic limit, which can be identified by the stress beyond which the material is no longer elastic or the deformation beyond which elasticity is lost. However, the change from elastic to plastic (non-elastic) behaviour is not always easy to define, and, approaching to the elastic limit, the stress-strain relation is no more linear: consequently, higher order terms in the strain tensor cannot be neglected and the new stress-strain relation may be written as

$$\sigma = E_1\varepsilon + E_2\varepsilon^2 + E_3\varepsilon^3 + \cdots \tag{2.14}$$

Nonlinear elastic behaviour may appear in many different ways (i.e. with or without hysteresis on the loading-unloading path), but in this work linear elastic behaviour is assumed and no further considerations on nonlinear elasticity will be given.

The elasticity of materials is described by the stress-strain curve (Figure 5), which shows the stress-strain relation during a uniaxial tensile stress test. The curve is linear for small deformations, and so Hooke's law can adequately describe the material behaviour and the slope of the curve is equal to the Young's modulus.

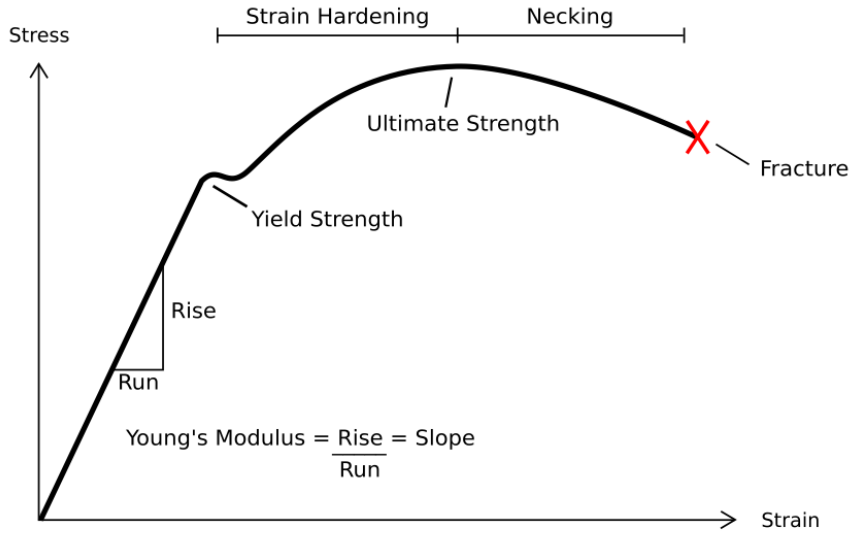

Figure 5: Representative stress-strain curve [4].

However, for stresses' values near the elastic limit, the relation is no longer linear and for even higher stresses, materials exhibit plastic behaviour deforming irreversibly and not returning to their original shape, after the stress is removed. The point where transition from elastic to plastic behaviour happens is the yield point.
Due to the wide variety of stress-strain curve exhibited by real materials, precise definitions of the yield point or of the elastic modulus are difficult to perform, and arbitrary definitions may be necessary (i.e. offset yield point for materials that not clear exhibit yield point).
Studying the materials response to static applied loads results in simplification on material behaviour, and in case of dynamic loading application more considerations are required.

2.2 Dynamic Mechanical Analysis

Dynamic Mechanical Analysis (DMA) is a method of material testing, which yields information on the mechanical properties under a small dynamic load as a function of time, temperature and/or frequency. The properties often investigated by DMA are the ability to lose energy as heat (damping) and the ability to recover from induced deformation (elasticity). A sinusoidal applied load, i.e. tension or deformation, results in a corresponding time dependent response signal – deformation or tension – regarding amplitude and phase shift: the resulting strain is also sinusoidal with the same frequency, but different behaviours may occur.
If a sinusoidal force is applied to an ideal elastic material, according to

$$\sigma = \sigma_0 \sin \omega t \tag{2.15}$$

the material response at any time may be written as

$$\varepsilon(t) = E \cdot \sigma_0 \sin \omega t = \varepsilon_0 \sin \omega t \tag{2.16}$$

representing a strain curve with no phase lag with the loading pattern.

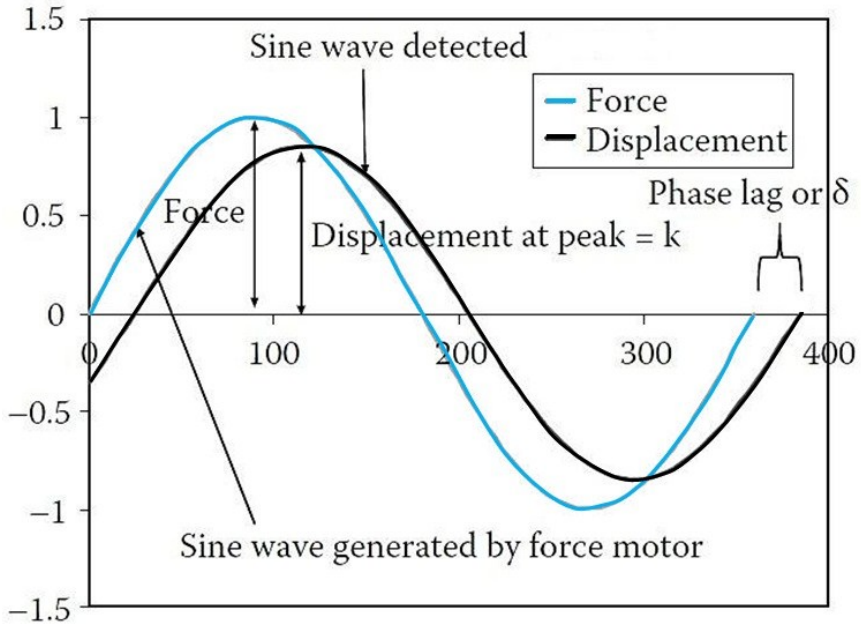

Figure 6: Example of DMA test [5].

An ideal viscous material will be responding according to

$$\varepsilon(t) = \omega\, \varepsilon_0 \cos \omega t = \omega\, \varepsilon_0 \sin(\omega t + \pi/2) \tag{2.17}$$

showing a 90° phase lag between stress and corresponding strain.

A common material will respond between these two limit behaviours, showing a phase angle δ (Figure 6).

The moduli measured in DMA are calculated from the material response to the sinusoidal wave: this leads to the definitions of the complex modulus E^* (or $G^*$and K^*, depending on the selected type of deformation). For instance, the time dependent Young's modulus E^* of a material being subjected to a strain at a frequency ω is a complex function which is expressed by:

$$E^*(\omega) = E'(\omega) + iE''(\omega) \tag{2.18}$$

Where E' is the storage modulus and represents the stress-strain ratio in phase with the strain (immediate elastic response); and E'' is the loss modulus and represents the stress-strain ratio out of phase with the strain (delayed response caused by energy dissipation).

The ratio of the loss modulus to the storage modulus is equal to $tan\ \delta$ (Figure 7):

$$\delta = \arctan\frac{E''}{E'} \tag{2.19}$$

and it is a measure of the ratio of dissipated energy to stored energy during a loading cycle, representing the mechanic damping or inner friction of a viscoelastic system.

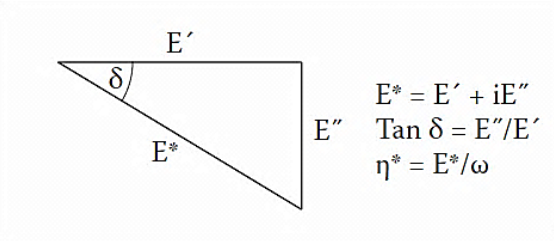

Figure 7: Representation of the relation between E*, E', E" and tan δ [5].

A high loss factor represents a high, non-elastic deformation part, a low loss factor a more elastic material.

DMA measurements can be carried out with stress (force) or strain (displacement) control; and DMA technique can be applied with all types of mechanical testing, such as three-point bending, tension, torsion or compression tests, with the corresponding geometries, but also creep or relaxation tests.
Physical properties can also be investigated, (glass transition, melting point, viscosity), studying their correlation with temperature variation, applied load velocity or frequency, and so on. Using special equipment features, tests in aggressive environment can be performed with DMA, and the adaptability of this technique to match real conditions is an obvious advantage on other types of experiments.

2.3 Poroelasticity

Poroelasticity is the continuum theory for analysis of the elastic behaviour of porous materials. In case a solid matrix is permeated by an interconnected network of pores, through which a fluid can move, poroelasticity describes the linked interaction

between fluid flow and porous media deformation. Rocks, soils and biological tissues are examples of this kind of materials. The presence of a free moving fluid affects the mechanical behaviour of the material: an increase of pore pressure determines dilatation of solid matrix, and compression of solid matrix causes the pore pressure to rise. The combination of these mechanisms gives new mechanical properties to the material, and the theory describing them is the Biot's theory [6], which in turn is inspired by Terzaghi's concept of "effective stress" [7].

Biot's theory is based on linear elasticity equations for the solid matrix, on Navier-Stokes equations (NSEs) for the fluid and on the Darcy's law for the laminar fluid flow.

The resulting material model is constructed as a coherent solid skeleton and a freely moving pore fluid, and it represents an idealized porous material, which is microscopically homogeneous and isotropic [2].

According to these hypothesis, is possible to identify two different types of displacement: the displacement of the porous solid and the motion of the fluid relative to the solid. Two strain quantities are also required to follow the deformations: the usual small strain tensor and the variation of fluid content. Of the two constitutive relations governing poroelastic behaviour, one relates stress, strain and pore pressure (p_p), modifying the classical linear stress-strain relation (2.4) in the following way:

$$\sigma_{ij}{}' = C_{ij}\varepsilon_{ij} - \alpha p_p \tag{2.20}$$

It means that the solid framework carries only the part $\sigma_{ij}{}'$ of the total stress σ_{ij}, while the fluid carries the remaining part αp_p: this is the concept of "effective stress".

The parameter α is an empirical constant named as Biot's coefficient, and it measures the change in pore volume relative to the change in bulk volume, at constant pore pressure. Thus, for a porous material, α has the property that if pore pressure is increased by a term δp, and all the normal stresses are decreased by $\alpha\delta p$, then there is no change in strain [8].

The other relation relates an increment in fluid content ζ to volumetric strain and to incremental pore pressure:

$$\delta\zeta = \alpha \cdot \varepsilon_{ij} + \frac{\delta p_p}{K_{eff}} \tag{2.21}$$

Where K_{eff} is the bulk modulus of the composite material (solid + fluid in the pores) and it is defined for ideal porous materials as:

$$\frac{1}{K_{eff}} = \frac{\alpha - \phi}{K_s} + \frac{\phi}{K_f} \tag{2.22}$$

Where ϕ represents the material porosity, K_s the solid matrix bulk modulus and K_f the fluid bulk modulus. An ideal porous material is one for which the porosity does not change under a total normal stress equal to the pore pressure.

Thus, the presence of pore fluid adds extra terms to stress-strain relations of the poroelastic material, and Biot demonstrated that ε_{ij}, ζ and dp_p are necessary to describe the stress-strain relations for this kind of materials [8].

Porous materials whose solid matrix is elastic and the fluid is viscous are poroelastic: porosity and permeability are peculiar properties of these materials.

Porosity ϕ is defined as the ratio of the pores volume to the total material volume and, assuming full saturation of connected pores space, the volume pore V_p can be substituted by the fluid volume V_f:

$$\phi = \frac{V_p}{V_t} = \frac{V_f}{V_t} \tag{2.23}$$

and consequently:

$$\frac{V_s}{V_t} = 1 - \phi \tag{2.24}$$

On the other hand, permeability k describes the ease with which fluids move through pores, and it is correlated to applied pressure, degree of saturation, density of fluid and its viscosity according to the Darcy's law.

Permeability's SI unit of measure is [m^2], but the practical unit is the darcy [D], and it is possible to assume:

$$1\ \text{darcy} = 9.86923 \cdot 10^{-13}\ \text{m}^2 \approx\ 10^{-12}\,\text{m}^2\ \approx 1\ \mu\text{m}^2 \tag{2.25}$$

Permeability is also function of the pore geometry and strongly dependent on porosity ϕ, and the estimation of permeability coefficient is a problematic challenge both from experimental and theoretical point of view. For instance, in an easy conceptual model of packing of spheres, and assuming laminar flow and low pore fluid velocity, a power law relation between k and ϕ exist, according to the Carman-Kozeny law [9]:

$$k \sim \phi^3/(1-\phi)^2 \tag{2.26}$$

An important aspect in the analysis of a fluid infiltrated porous material is the difference between drained and undrained deformation: the undrained response happens when the fluid is trapped in the porous solid such that $\zeta = 0$, while the drained condition corresponds to zero pore pressure $p_p = 0$. Under both drained and undrained conditions, a poroelastic material behaves as an elastic one, the undrained material being however stiffer than the drained one [10].

2.4 Navier-Stokes equations and Darcy's law

A brief description of Navier-Stokes equations (NSEs) and Darcy's law is presented, as they represent the governing equation for the fluid motion in the Biot's theory regarding poroelastic materials.

NSEs are nonlinear partial different equations describing the motion of fluids, dictating velocity rather than position. After the velocity field is solved for a particular point at a certain time, other quantities may be solved. With certain hypothesis, they can be simplified to linear equations.

Assuming that the fluid is incompressible (fluid density does not change with the pressure) and Newtonian (viscosity is constant and does not depend on the stress state and velocity of the flow), the general form of NSEs is [11]:

$$\rho \frac{\partial u}{\partial t} + (\rho u \cdot \nabla) u = -\nabla p + \nabla \cdot (\mu (\nabla u + (\nabla u)^T)) + F \tag{2.27}$$

The equation derives from the combination of mass conservation, momentum conservation and energy conservation.

Darcy's law is a constitutive equation that describes the fluid flow through interstices in a porous material; Darcy's law applies when the gradient in hydraulic potential drives fluids movement in the porous medium. According to it, the relationship between the change rate through the medium, the fluid viscosity and the pressure drop over a given distance is simply proportional:

$$U = -\frac{k \cdot A}{\mu} \frac{(\Delta P)}{L} \tag{2.28}$$

Where U represents the fluid flow rate, units of volume per time [m^3/s], A is the cross sectional area to flow [m^2]; μ is the dynamic viscosity of the fluid [Pa·s]; L is the considered length and ΔP is the total pressure drop. As others flux laws, such as Fourier's, Ohm's and Fick's law, the negative sign is necessary because fluid flows to the opposite direction than the gradient.

Focusing from macro scale to micro scale, Darcy's law states that the velocity field is determined by the pressure gradient, the fluid viscosity and the structure of the porous medium [11]:

$$\boldsymbol{u} = -\frac{k}{\mu} \frac{\partial p}{\partial x} \tag{2.29}$$

Where **u** represents the specific discharge [$m \cdot s^{-1}$] across the sectional area. If gravity cannot be neglected, a potential term ($\rho \cdot g \cdot \partial z$) has to be added, but it is possible to set z as zero if the flow is entirely horizontal within the *xy*-plane.

Considering that only a fraction of the volume (or the area) is available for flowing, the Darcy fluid velocity u_D [m·s^{-1}] is related to the specific discharge by the porosity, according to:

$$u_D = \frac{\boldsymbol{u}}{\phi} \tag{2.30}$$

Usually fluids typically occupy only a part of the porous volume, so it follows that velocities within the pores are higher than Darcy velocity, according to:

$$u_r = \frac{u_D}{\theta_s} \tag{2.31}$$

Where θ_s is the fluid volume fraction [-]. For saturated system, θ_s equals the porosity.

Darcy's law is valid only for low-velocity viscous flows; it can be applied to any flow with Reynolds number up to 10. Reynolds number *Re* is a dimensionless parameter that represents the ratio of the inertial forces F_i to viscous forces F_v aging on a fluid particle, and it is expressed as:

$$Re = \frac{F_i}{F_v} = \frac{\rho \cdot \boldsymbol{u} \cdot d}{\mu} \tag{2.32}$$

Where ρ is the density of the fluid and d is the equivalent diameter of the duct. At low Reynolds numbers, viscous forces dominate and tend to damp out all disturbances, leading to laminar flow; at high Reynolds numbers, small disturbances have the possibility to grow by nonlinear interactions, ending up in a chaotic, turbulent state. However, fluid loses considerable energy to frictional resistance within pores, so flow velocities in porous media are very low and the application of Darcy's law is reasonable.

The Darcy's law solution is practically to find for pressure p. Inserting (2.29) into the equation of continuity (2.33) produces the generalized governing equation, which can be used to solve poroelasticity problems:

$$\frac{\partial p}{\partial t}(\rho\, \theta_s) + \nabla \cdot \rho\, \boldsymbol{u} = \rho\, Q_s \tag{2.33}$$

Leading to:

$$\frac{\partial p}{\partial t}(\rho\ \theta_s) + \nabla \cdot \rho \left[-\frac{k}{\mu}\ (\nabla P + \rho\ g\ \nabla D) \right] = \rho\ Q_s \tag{2.34}$$

The Darcy's law assumes that the fluid is incompressible so that ρ is constant, so the equation can be further simplified.

The solid mechanics and fluid mechanics concepts presented in this chapter are preparatory to the next chapters, in order to understand the requirements that biomaterials have to accomplish, especially in orthopaedic applications, where mechanical properties play an important role, but the interactions with the surrounding environment (living cells, fluids…) cannot be neglected.

3 INTRODUCTION TO BIOMATERIALS

3.1 Definition of a biomaterial

As the biomaterials field represents the meeting point of different knowledge fields, requiring a multidisciplinary approach between medicine, chemistry, engineering and biology, it is necessary to introduce some basic definitions.

The formal definition of a biomaterial is commonly expressed as a "synthetic material used to replace part of a living system or to function in intimate contact with living tissues [12] and body fluids [13], for a short term or for the entire life of the host". It's possible to give also other definitions of biomaterial, i.e. "a systematically and pharmacologically inert substance designed for implantation within or incorporation with living tissue" **Errore. L'origine riferimento non è stata trovata.**, or "a material used to make devices to replace a part or a function of the body in a safe, reliable, economic and physiologically manner" [12]. All these designations exclude materials used for devices such as surgical instruments or for external prostheses such as artificial limbs or hearing aids: latters are not in contact with body fluids, and the previous do not replace any function of human tissue.

It is assumed that biomaterials are also biocompatible, which is "the ability of a material to perform with an appropriate host response in a specific application" [15]. However, biocompatibility is a very complex parameter of how the body interacts with the biomaterial during the implant life term. Introducing a foreign object in a living body causes the natural reaction of the host's immune system, which is to avoid in order to guarantee the success of the artificial device. In general, is possible to classify a biomaterial by the tissue response it causes: biotolerant, bioinert and bioactive materials are identified.

Biotolerant materials release substances but in non-toxic concentrations and lead to benign tissue reactions; bioinert materials exhibit minimal chemical interactions with living tissue; bioactive materials show a positive interaction with surrounding tissues, encouraging healing, chemical bounding or load transmission.

Furthermore, even without the immune system's response, a living body is not a comfortable environment for a common material: the interaction with flowing fluids,

living cells and free ions can lead to material modifications (i.e. premature corrosion) and the consequent failure of the implant, or can provoke irritations and diseases of the surrounding tissues or of the entire body.

Therefore, a biomaterial has to embody many special characteristics in order to reach biocompatibility and perform its function without failure:

- promote healing
- not provoke tissue irritation or inflammation
- not contain toxic, allergic or carcinogenic elements
- be relatively inexpensive, easy to be processed and even replaced or recycled
- be biocompatible and biofunctional for its lifetime in host
- be stable during time and avoid wear or corrosion

The last of these characteristics is not applicable for the case of self-resorbable devices, like stitches, sutures, clips or any other device which doesn't need any surgical operation to be removed.

3.2 Biomaterial Classes

Focusing on the material engineering point-of-view, it's possible to categorise biomaterials in the typical material classes, such as metals, polymers, ceramics and composite materials.

Each one of these classes has its applications, its pro and con, its typical behaviour and requirements. Let's briefly reassume the salient features of each class:

- Metals: due to their suitable mechanical and fatigue strength, they are involved in structural application, such as bones recovery or replacement. Their handicaps are high density, risk of corrosion and consequent hazard for health care. Because of this, only stainless steels, CoCr alloys, Ti alloys and few others alloys are used in biomedical applications [16].
- Ceramics: their high compressive strength, combined with medium density and commonly high biocompatibility are the most important advantages of this class; their main applications are found in dental surgery and hip replacements. On the other hand, high production costs and processing

difficulties are the main problems to deal with. Alumina and yttria stabilized zirconia are the most used materials for implants, with a large variety of glasses used as coatings[12].

- Polymers: they have low density, high biocompatibility, low cost and are easy to process, but they also have low modulus and poor mechanical characteristics, which limit their applications. Common polymers for orthopaedic applications are acrylic, nylon, silicone, polyurethane, polypropylene and ultra high molecular weight polyethylene [17].
- Composites: they are hard to design and process and because of this very expensive, however they have many applications and extensive literature exist in composite materials field, which has very concrete possibilities of future developments, including composites with biological macromolecules [18].

Such materials are used in wide variety of form, such as moulded or machined parts, fibers, films and coating, membranes, foams or fabrics.

The characteristics of the environment in which an implant has to operate and function it has to perform set the boundary condition for the implant design. In any case, the designer will conduct a material selection process, first, among the generic classes and, secondly, within a given generic class [16], in order to achieve the best performance in terms of biofunctionality.

In material science of bone substitution biomaterials there are two main issues: mechanical properties and biocompatibility.

A bone implant should guarantee an identical response to loads and stresses as real bone. For instance, the load on a hip joint is estimated to be up to three times body weight, and the peak loading can reach level as high as 10 times body weight. Moreover, a cycling loading as high as 10^6 cycles in 1 year [19] has to be performed in an inhospitable environment for foreign bodies, such as the human body is. For instance, every year only in US 300’000 patients receive a total hip replacement (THR) surgery [1]. Despite human hip joint is subjected to high levels of stress and high number of loading cycle, with the latest improvements ambulatory function can be restored within a short time. However, under such loading conditions, most

implants must be replaced after 15-20 years: it is estimated that 20% of hip surgeries replace the original failed implant [20].
Fatigue, crack propagation, wear and abrasion or bone loosening are just few of the possible origins of implant failure.
Taking into account the complex nature of the problem, it is understandable why engineered biomaterials with optimal combination of biocompatibility, tensile strength, fatigue strength and fracture toughness are necessary for implant design and its successful application.
Furthermore, other properties have to be considered: unsuitable magnetic or acoustic properties could adversely affect the results of subsequent diagnostic methods, such as ultrasonic monitoring or MRI radiography.

In this work, for understanding peculiarities of biomaterials used for bone replacement (hard tissue replacement), biomaterials properties and requirements have to be considered taking into account bone tissue environment, which will be presented in the next chapter, primarily focusing on bone mechanical properties.

4 BONE STRUCTURE AND PROPERTIES

Bone is a composite material made up of collagen fiber matrix (the organic phase), stiffened by hydroxyapatite ($Ca_{10}(PO_4)_6(OH)_2$) crystals (HAP). Other minerals, proteins and polysaccharides are also present in bone. A rough approximation for overall composition by volume is one-third HAP, one-third collagen and other organic components, and one-third water [21].

Microscopically, the fundamental structure unit of bone is the osteon, or haversian system, composed of concentric layers of mineralized matrix surrounding a central canal containing blood vessels and nerve fibers [22].

Bone is histologically divided in immature woven bone (trabecular) and mature lamellar bone (cortical). The collagen in woven bone is fine fibered and randomly oriented, and the woven bone consists of cells and blood vessels. In cortical compact bone, collagen forms branching bundles and lamellae are circumferential layers around a central canal, which contains blood vessels [23] (Figure 8).

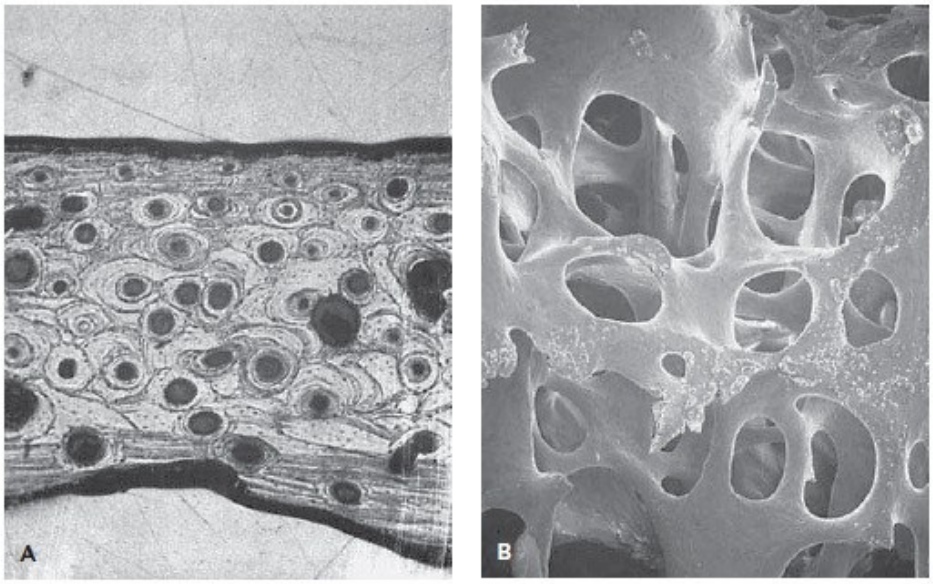

Figure 8: A) Photomicrograph (x40) of human cortical bone and B) Scanning electron photomicrograph (x30) of human trabecular bone [22]

Cortical bone is stiffer than trabecular bone, withstanding greater stress but less strain before failure: because of its porous structure, cancellous bone has great

capacity for energy storage and can sustain up to 50% of strain before yielding, whereas cortical bone yields and starts to fracture for strain over 1.5% - 2% [22].
Reported literature properties of bone are found to vary, but these differences come mainly from the biological origin of bone and consequently they depend on factors such as the individual state of health or age, level of physical activity and the part of the body from which the bone is coming. In fact histology of a bone is strictly related to its function in the body [23].
Bone is an anisotropic, heterogeneous, inhomogeneous, nonlinear and viscoelastic material [21].

4.1 Strength and elastic/plastic deformation

Bone density is one of the most important factor in determining the elastic properties: they increase as bone density increases [24].
The elastic modulus of a bone is intermediate between that of HAP and collagen; but the total strength is higher than that of both. HAP is quite brittle with poor impact resistance and fractures easily, however, bone properties come from the combination of the high hardness of HAP and the high fracture toughness of the organic phase.
Ultimate tensile strength of human compact bone in direction parallel to osteon is about 150 MPa (Table 1) [25]. Considering that the criterion for structural strength in beam bending is the material strength divided by the 1.5 power of density, the strength to density ratio for bone is greater than that for equivalent structural steel [26].

Table 1: Properties of long human bone [16], [22].

	Young's Modulus [GPa]	**UT Strength [MPa]**	**Fatigue Strength [MPa]**
parallel tensile	14-22	100-150	30
parallel bending	4	157-181	-
perpendicular tensile	-	10-50	-
perpendicular bending	-	106-130	-

However, bone is highly anisotropic and when transversely loaded it is not as strong as along osteon parallel direction, and considering each type of load that a bone can experience (tension, compression, bending, torsion, shear and any combination of them), is it possible to understand the different categories of bone failure.

Bone when loaded exhibits a yield point ($\sigma_y = 114\ MPa$ according to [27]), but the yield mechanism is the result of microcracking and damages, differently from the usual metal mechanism by motion of dislocation.

Loading of bone in vivo is a complex mechanism because there are multiple indeterminate loads and geometric structure of bone is irregular: the complexity of loading pattern during walking or jogging is demonstrated by in vivo measurement (Figure 9).

Thus, at the quasi-static strain rates in mechanical testing and in common human activities, it is possible to approximate the cortical bone as an anisotropic, linear elastic material [21] following the generalized form of Hooke's law (2.4).

Two different types of anisotropic behaviour are suitable to describe the bone loading response: orthotropic behaviour or transverse isotropic behaviour [28].

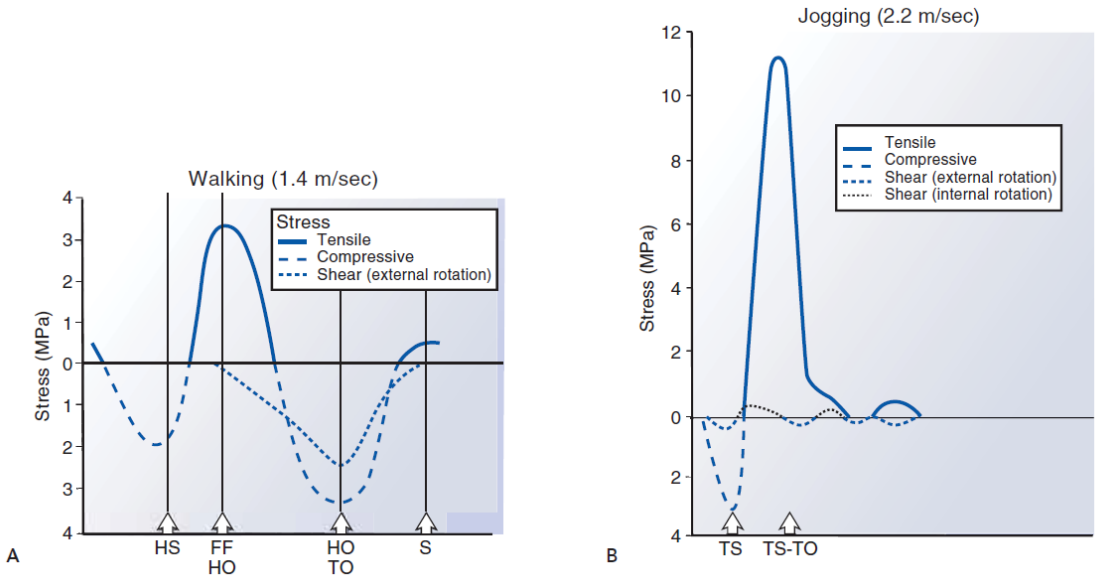

Figure 9: A) Calculated stresses on walking tibia. HS: heel strike; FF: foot flat; HO: heel-off; TO: toe-off; S: swing. B) Calculated stresses on tibia during jogging. TS: toe strike; TO: toe-off [22].

Tests for investigating elastic properties of bone can be carried out with classical mechanical tests (tensile loading, three-points bending, etc.) or by wave propagation techniques: the latter are preferable because better reproducibility is performed and redundant measurements on the same specimen are achievable, with the possibility to characterize mechanical properties along whatsoever direction [21].

4.2 Fatigue and stress concentrations in bone

As bone does not exhibit endurance limit (no asymptotic plateau in its typical fatigue curve), it accumulates fatigue damage during life, and biological bone remodelling is essential for structural integrity of skeletal system.

Bone is the only hard tissue able to undergo spontaneous regeneration and to remodel its micro and macro structure, and this is accomplished through a delicate balance between an osteogenic and osteoclastic process, influenced by static and dynamic stresses applied to bone.

This ability is described by the Wolff's law [29], results that the new bone structure is adapted to the applied stress, by altering size, shape and density of bone. Thus, a bone subjected to dynamic loading regenerates and bone not subjected to loading results in atrophy.

Obviously, the time in which a given number of load cycling are applied must not be shorter than time for bone remodelling process to prevent failure (typically three months after a change in activity routine) for that range of load, because a fatigue fracture can result when the remodelling process is outpaced by the fatigue process. Cracking or fracture of bones due to fatigue are clinically called as "stress fractures".

Thus, the fatigue process for bones is affected also by the number of applications of the load within a given time, namely by loading frequency.

Figure 10 represents bone's nonlinear dependence on load intensity and cycle number in the maintenance of bone health: any point in the region above the optimal ratio of load intensity to cycle number is anabolic, whereas any point in the region below leads to resorption.

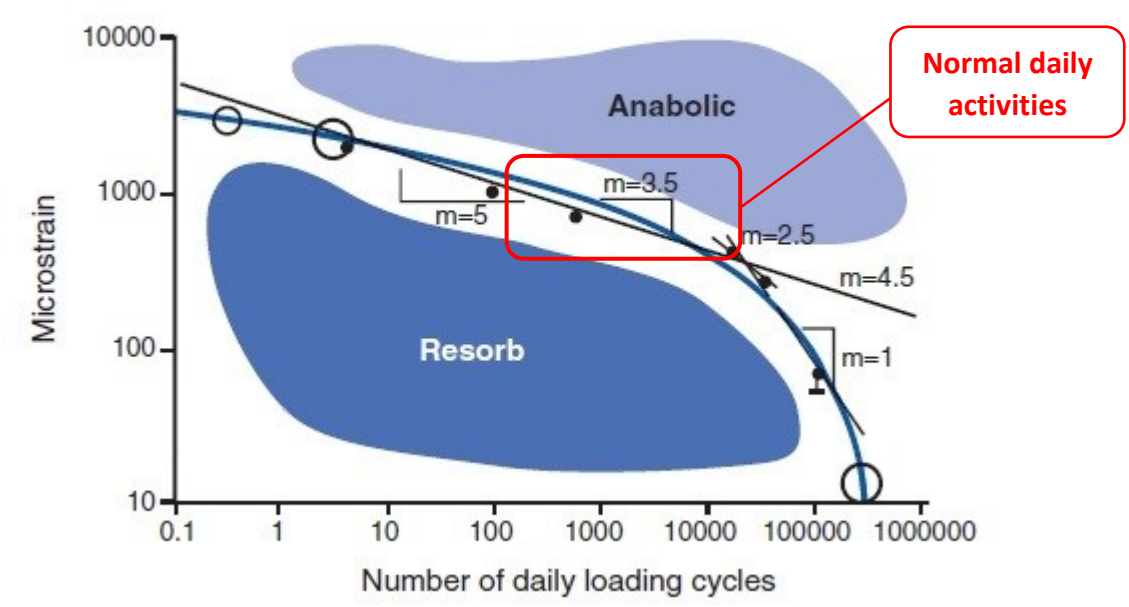

Figure 10: Fatigue process of bone is influenced also by loading frequency [22] .

Fatigue resistance of bone is controlled by strain range, and it decreases during life, because bone density and elastic modulus increase with age. Strain leading to microdamage is between usual strain $(400 - 1500\ \mu\varepsilon)$ and strain causing failure $(10000\ \mu\varepsilon)$ [22]. In vivo activities, the maximum strain recorded for human tibia was about 8000 microstrain during running [30].

Toughness is another important characteristic of bones: it represents the response to the microcracks occurring during life and describes the fracture behaviour. Fracture toughness and energy adsorbed to fracture decrease during childhood, while elastic modulus and stiffness increase monotonically during age [31]; furthermore the fibers pull-out seems to be an operative toughening mechanism [23].

Holes and notches have less influence on bone resistance than expected, and this happens because the bone already experiences stress raisers because of its heterogeneous structure and porosity [32]. Thus, stress concentration around holes are less than the ordinary predicted value and the strength seems to be independent from notch sharpness [33]. However, further stress raisers are introduced with surgery, such as when bone pieces are removed or screws are inserted. The weakening effect of stress raisers is mostly noticeable under torsional loading, but

bone remodelling is able to restore the normal strength of the bone in 8-10 weeks [32].

4.3 Viscoelasticity

Bone exhibits viscoelastic behaviour, meaning the stress depends not only on the strain, but also on the rate at which the load is applied: bone is stiffer when loads are applied at higher rates and can store more energy before failure [22]. However, bone becomes more brittle for very high strain rates, which represent traumatic impact (Figure 11).

Mechanical behaviour of a viscoelastic material depends also on the time history of strain. In case we study the bone being subjected to a strain at a frequency ω, the time dependent Young's modulus E^* is expressed by (2.18).

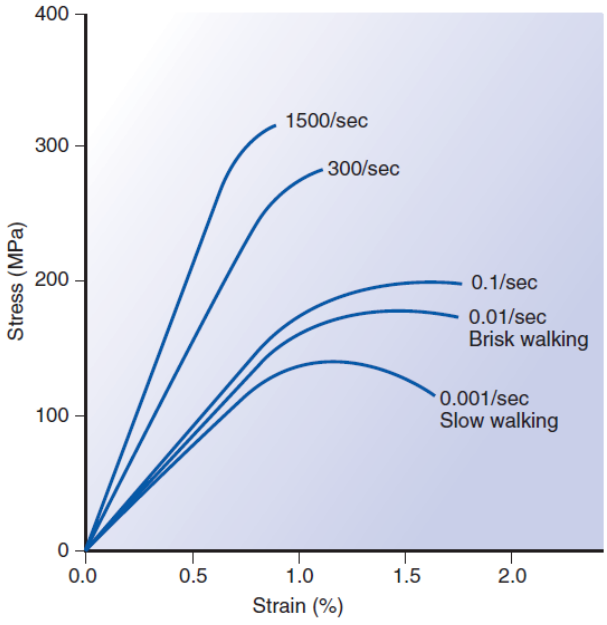

Figure 11: Stress-strain rate dependency of bone [22].

In bones, loss tangent $\tan\delta$ achieves a minimum value of ~ 0.02 at frequencies between 0.1 and 100 Hz (Figure 12), which is the typical range for common human activities[34].

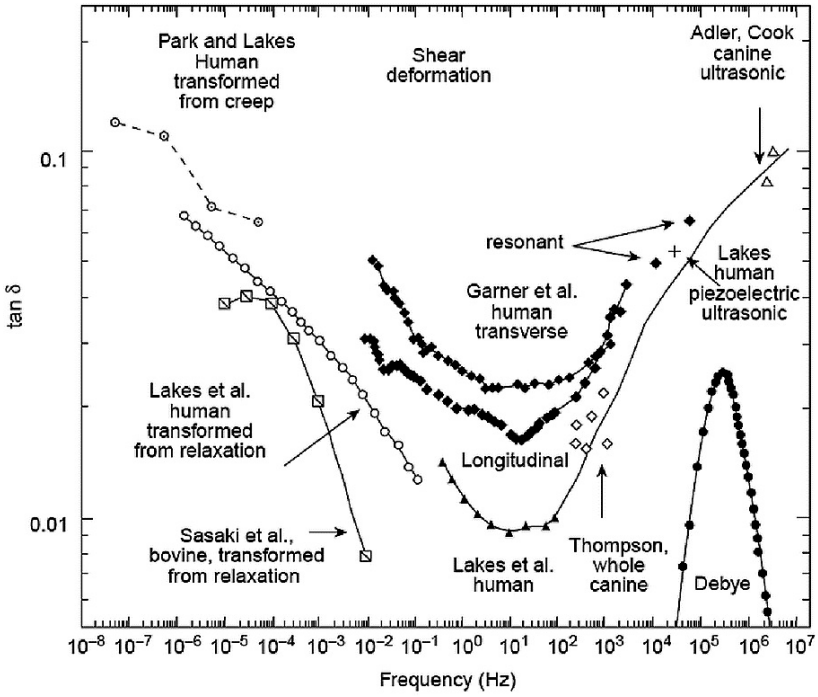

Figure 12: Dependency of tan δ on loading frequency of compact bone, according to different experimental tests [35].

The bone is a bio-nano-composite system with optimized properties: its properties are due to its structure and many attempts to simulate bone structure with composite models were done in past years, and conventional anisotropic elasticity has been shown to be entirely adequate.

Substitute a broken bone or a perished joint with an artificial device is the main challenge of orthopaedics.

Metals are the most important materials in this particular fields, and in the next chapter a brief introduction on metals as biomaterials anticipates the main part of this literature review, that is the discussion on titanium as biomaterial and on its requirements as the best material available for orthopaedic device .

5 METALS AND TITANIUM AS BIOMATERIALS

Metals, which can be used as biomaterials, are suited to almost every kind of loading and those showing a fatigue limit are the best candidates to perform the role as living tissue substitute, being able to maintain desired characteristics during time, without losing performance or functionality. Furthermore, metals may have unique properties suited for special application, such as silver bactericidal properties, gold inert behaviour or nickel-titanium shape memory effect (SME).

In history of orthopaedic prosthesis, metals represent the main resource from which the practice of implant systems began.

As mentioned before, a biomaterial works in close contact with living tissues and fluids: this means metal selected as biomaterial has to guarantee his performance in a hostile environment and to perform its function without negative collateral effects.

Considering their wide range of mechanical properties, is possible to classify metals in two main groups:

- metals for low-loaded implants (such as plate and screws)
- metals for high-loaded implants (i.e. hip and knee prosthesis)

First attempts to repair broken bones started in 1930s with vanadium steels used to manufacture bone fracture plates and screws: their poor corrosion resistance allowed their use only for temporary implants.

In 1940s were introduced austenitic 18/8 (302 according to the ASTM classification) stainless steels (SS); later types 18/8Mo and 18/8Mo low carbon (respectively 316 and 316L type) SS become available: addition of Mo improves resistance to pitting corrosion. This feature made them the preferable choice, but not suited enough for permanent implants.

New developments were made with CoCr alloys, especially with types Co29Cr5Mo (known as ISO 5832-VII or ASTM F75) and Co20Cr35Ni10Mo (known as ISO 5832-VI or ASTM F562).

Both of them have better fatigue performance and ultimate tensile strength than SS, but especially have high corrosion resistance under stress, which allows them a long service life without crack initiation or stress fatigue. Disadvantages are their high

density and their high elastic modulus, which may have bad implications with load transfer and bone health.

Meanwhile, from late 1930s, has become widespread the use of commercially pure (cp) titanium with its four different ASTM grades and the use of Ti6Al4V (ASTM F136) alloy for implants manufacturing, due to their lightness and their suitable mechanical and chemical properties.

Density of Ti-alloys is about 4.5 g/cm^3 and lies between that of Al-alloys and steels, and it is half the density of CoCr or CoNiCr alloys (Table 2). Moreover, cp Ti has the same ultimate tensile strength (UTS) of a common low-grade steel alloys (440 MPa) but is 45% less dense; on the other hand, Ti is 60% more dense than aluminium, but more than twice as strong as 6061-T6 aluminium alloy.

According to this, it is understandable why Ti-alloys are a good choice for human implants, but these aspects will be discussed in following paragraphs.

Table 2: Basic properties of metallic implant alloys, [12],[16].

Alloy	Density [g/cm^3]	Tensile Strength [MPa]	Young's Modulus [GPa]
316 stainless steel	7.9	850	210
CoCrMo alloys	8.3	600	220
CoNiCrMo alloys	9.2	950	220
Ti and Ti alloys	4.5	900	110
NiTi alloy	6.7	800	75

5.1 Commercially pure titanium and Ti-alloys:

Ti is the 22th element of the periodic table, a transition metal from the d-block, with low density and high strength. It was first identified as a new metallic element by Gregor in 1791 and named Titanium in 1795 by Klapproth. Despite Ti is the ninth-most abundant element in the Earth's crust and the seventh most abundant metal, it is always chemically bonded to other elements (as occurs in minerals like rutile, ilmenite, perovskite or anatase) and was not until the middle of the 20th century that W.J. Kroll developed a new commercially attractive process in Luxemburg (1940) to

extract metallic titanium from its minerals. The Kroll process will be discussed in the following chapter.

In its metal form titanium is used in light alloys; its oxide (TiO_2) is the most important component of white pigments.

Due to their high tensile strength to density ratio, high corrosion resistance, fatigue resistance and ability to withstand moderately high temperatures without creeping, Ti alloys find applications in advanced scientific fields, such as aerospace and automotive, military and industrial processes, medical prostheses, dental and orthopaedic implants, jewellery and sport equipment.

Most of the commercial applications are for chemical and petrochemical industries (such as tubes, liners, heat exchangers…), as alternative to stainless steels, Inconel or Monel alloys: because titanium is usually more expensive, its choice is based on its life cycle cost and its longer durability. Because of this, Ti is available into the general consumer market only for high-end products.

Thanks to the high yield stress value that can be tolerated from Ti-alloys, they are the best choice where weight saving is a critical factor: Ti-alloys strength-to-density ratio (especially in the 200-450 °C range) is the highest in the entire metal category. It has a relatively high melting point (1668 °C), low electrical and thermal conductivities and non-ferromagnetic behaviour.

Titanium is an allotropic material, which can have a hexagonal close packed crystal structure (α-Ti, hcp) or a body-centered cubic crystal structure (β-Ti, bcc) above 882.5 °C, which remains stable to the melting temperature. Obviously, the exact transformation temperature is influenced by interstitial and substitutional elements. For pure α-Ti the resulting ratio c/a is equal to 1.587, smaller than the ideal ratio for a hexagonal closed packed crystal structure with $c/a = 1.633$ (Figure 13).

The intrinsic anisotropic behaviour of the hexagonal crystal of the α-phase has important consequences for elastic and plastic deformation behaviour of titanium and its alloys. Because of this, Young's modulus and shear modulus vary as a function of the angle γ between the c-axis of the unit cell and the applied stress axis.

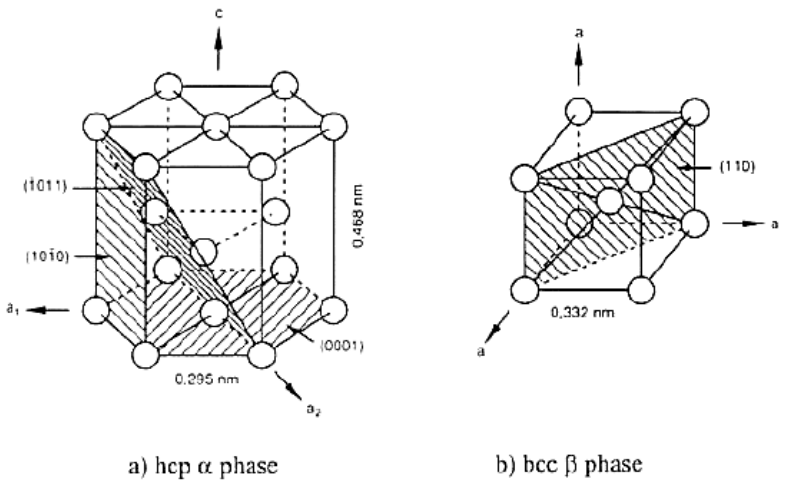

Figure 13: Unit cells of α and β phases [36]

The elastic moduli are decreasing almost linearly with increasing the temperature up to the transformation temperature: for polycrystalline α-Ti Young's modulus drops from about 100 GPa at room temperature to about 58 GPa below transus temperature, while the shear modulus decreases from 42 to 20 GPa (Table 3).

Table 3: Physical properties of cp-titanium [16].

Property	**Value**
Young's modulus at 20 °C	100-145 GPa
Shear modulus at 20 °C	34-46 GPa
Poisson's ratio	0,33
Density	4.51 $kg \cdot m^{-3}$
Melting temperature	1668 °C
Transformation temperature	882.5 °C
Cristal structures	>850 °C β bcc <850 °C α hcp
Magnetic properties	Paramagnetic
Heat of transformation	67 $kJ \cdot kg^{-1}$
Specific heat at 15 °C	523 $J \cdot kg^{-1} \cdot K^{-1}$
Heat fusion	419 $kJ \cdot kg^{-1}$
Thermal conductivity at 20 °C	15 $W\ m^{-1} \cdot K^{-1}$
Thermal expansion coefficient between 20 - 200 °C	$8{,}36 \cdot 10^{-6}\ K^{-1}$
Specific electrical resistivity at 20 °C	0.56 μΩ·m

Since the β-phase of pure Ti cannot be retained at room temperature, it's possible to measure the moduli only for binary β-Ti alloys: the moduli of β-Ti increase with increasing the solute content, but their values are lower than those of α-Ti.

The transformation of the bcc β-phase to the hcp α-phase by cooling down occurs by a nucleation and shear type process, which can lead to martensitic process or a nucleation and growth process, depending on composition and cooling rate.

Quenching of the bcc β-phase can lead to two different crystal structures: hexagonal martensite α', or orthorhombic martensite α''. Hexagonal α' can exist in two microstructural morphologies: massive martensite (high purity Ti or dilute alloys), and acicular martensite (alloys with higher solute content). Orthorhombic α'' occurs in Ti-alloys with β-stabilisers and in Al+V compositions.

In Ti-alloys with medium solute content, cooled with sufficiently low rates, nucleation of α at β grain boundaries occurs: the resulting microstructure consists of colonies of parallel α plates separated by plates of retained β phase.

In addition to the just mentioned titanium physical properties, one of the most important characteristic of titanium and Ti-alloys is their high corrosion resistance. Titanium metal and its alloys oxidize immediately upon exposure to air, forming a dense oxide coating that protects the bulk form further oxidation.

The driving force for quick oxidation of Ti is the great chemical affinity between Ti and oxygen, together with the high maximum solubility of oxygen in Ti of about 14.3 wt.%, which causes the formation of a highly oxygen enriched layer under the oxide layer, called "α-case". The α-case is less ductile and can cause early crack nucleation under fatigue bending: this allows the application of common Ti-alloys to regime temperature only below 550 °C, where the diffusion rates through the oxide layer are low enough to prevent oxygen being dissolved into the bulk. Due to this oxide coating, Ti exhibits great resistance to corrosion, but as indicated by its negative redox potential, titanium is thermodynamically a very reactive metal, which burns before its melting point: melting is possible only in inert atmosphere or vacuum. Nitrogen acts in the same way to give a coating of nitride. Titanium has also the capability to assume different attractive colours when anodized and varying the thickness of surface oxide layer causes interference fringes.

Titanium shows different behaviour depending to the different alloying elements. which can be classified in substitution elements (V, Ta, Nb), interstitial elements (O and N), precipitation hardening promoting elements (Cr, Mn, Fe, Co, Ni…).

All elements which are within the range 0.85-1.15 of the atomic radius of Ti can alloy substitutionally and have significant solubility in titanium; elements with an atomic radius less than 0.59 of Ti occupy interstitial sites (such as H, N, O, C, B).
Alloying elements can be categorised according to their effect on the stability of the α-phase or on the α to β transformation temperature (Figure 14).

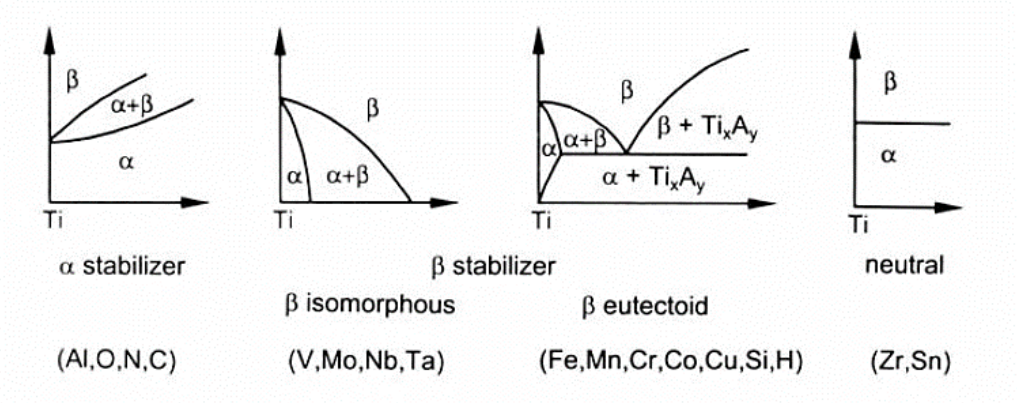

Figure 14: Effect of elements addition on equilibrium phase diagrams of Ti-alloys [36].

Thus, Al, O, N and C are all α-stabilisers and increase the transformation temperature with increasing the solute content; Mo, V, W, Nb and Ta are β-isomorphous stabilisers; Cu, Mn, Fe, Ni, Co and H are also β-stabilisers but form eutectoid structures. The eutectoid reaction is usually slow and it is frequently inhibited. Mo and V have the largest influence on β stability and are the most common alloying elements. Zr and Sn are neutral alloying elements.
Commercial Ti-alloys are classified in three different categories: α, α+β and β alloys, according to their equilibrium microstructure. The ASTM standards recognize 31 grade of Ti metal and alloys. Grade 1 thought 4 are commercially pure Ti (Table 4), distinguished by their increasing values of UTS as a function of oxygen content, ranging from 1800 to 4000 ppm. The most widely used Ti alloy is the grade 5, known also as Ti6Al4V from its composition (Table 5).

Table 4: Chemical composition (wt%) of cp-titanium [16].

	Ti	**Fe**	**O**	**N**	**C**	**H**
Grade 1	Balance	0,2	0,18	0,05	0,08	0,013
Grade 2	Balance	0,25	0,25	0,06	0,08	0,013
Grade 3	Balance	0,3	0,35	0,06	0,1	0,013
Grade 4	Balance	0,35	0,40	0,07	0,1	0,013

Table 5: Chemical composition (wt%) of (α+β)-titanium alloys [16].

	Ti	Al	V	Fe	Nb	Ta	O	N	C	H
Ti6Al4V	Balance	6,75	4,5	0,3	-	-	0,2	0,05	0,08	0,015
Ti5Al2.5Fe	Balance	5,5	-	3,0	-	-	0,2	0,05	0,08	0,015
Ti6Al7Nb	Balance	6,5	-	0,25	7,5	0,5	0,2	0,05	0,08	0,009

Cp-Ti and α-alloys take advantage for heat treatment and forging from the presence of a small amount of the more ductile β-phase. Aluminium is the main alloying element apart from Zr and Sn, and α alloys are strengthened by substitutional atoms, and suitable heat treatments allows the precipitation of α'' particles, coherent with the α matrix, providing an extremely high hardening effect.

Metastable β alloys have high content in β stabilisers, but isothermal aging can lead to α+β structure. There are two known main metastable phases, ω and β'. The ω-phase is observed in alloys with medium β stabilisers contents during aging process up to 550 °C, and it is coherent with the β matrix. It serves as nucleation site for α phase if aging is extended. The β'-phase is observed between 200-500 °C in alloys with enough β stabilisers to preclude the ω-phase transformation and where the direct transformation α > β is slow. Similarly to the ω-phase, it act as nucleation sites for α-phase formation. The precipitation of ω-phase (composed of Ti and β-stabilising elements) can provoke local enrichment of V (highly toxic) up to 20-25%: because of this have been developed alloys such as Ti5Al2.5Fe or Ti6Al7Nb, without toxic elements.

Compared with β ones, α-alloys show higher resistance to plastic deformation and lower ductility, more anisotropic behaviour and better creep resistance [37]. The α+β alloys usually have high strength and formability, and contain 4-6% of β-stabilisers which allow some amounts of β to be retained on quenching from the β to the α+β phase fields. Ti6Al4V is the most common alloy of this type, due to its high strength (1100 MPa), creep resistance at 300 °C, fatigue resistance and castability.

Fatigue strength is defined as the highest periodic stress that does not initiate a failure of the material after a given number of cycles. Thus, fatigue strength is lower than the yield strength, which corresponds to a single loading cycle. Fatigue strength is dependent on the type of applied load: it can be, for instance, tension-compression

(σ_f) or rotating bending (σ_R). The stress ratio R is the ratio of the lowest to the highest applied stress amplitude. K is a factor concerning the material resistance to crack propagation, and failure occurs when K reaches the critical value K_C, which is the plane stress fracture toughness. K is dependent on the loading mode, and in mode I the load is applied perpendicular to an initiated crack (K_{IC}).
Ti alloys fatigue limit is shown in Table 6 [38].

Table 6: Mechanical properties of cp-Ti and Ti alloys [16].

Alloy	**Tensile Strength UTS [MPa]**	**Fatigue Strength σ_f [MPa] (R=1)**	**Rotating-bending fatigue strength σ_R [MPa] (R=1)**	**Fracture toughness K_{IC} [N·mm$^{-3/2}$]**
cp-Ti grade 3	450	230-280	200	-
Ti6Al4V	920-1140	400-450	500-660	1740-2020
Ti5Al2.5Fe	860	-	450-550	1225-1785
Ti6Al7Nb	870-1000	-	450-600	-
Ti30Ta	-	-	400	-
Ti12Mo6Zr2Fe	1060-1100	410	585	3880
Ti13Nb13Zr	700-1030	425-500	-	2150

On the other hand, Ti and its alloys show some disadvantages. One of them is their poor shear strength and their tendency to gall or seize when in sliding contact.
Ti alloys have also poor cold deformability due to the precipitation hardening of secondary phases, but when cold deformation is carried out, it can guarantee a fine-grained microstructure: the grain of different phases hinder each other in their growth.
Furthermore, its price is also higher than the other metals usually used and this is due to the difficulty to extract metallic Ti from its minerals: the process is still expensive and limits the further application of Ti alloys.

5.2 Titanium production and processing:

5.2.1 Obtaining Titanium metal

Early stages of material production may have a large impact on the raw material quality. The main process to produce metallic titanium is the recently Kroll process. There titanium metal is obtained by reduction of titanium tetrachloride ($TiCl_4$), which is made by chlorinating rutile (TiO_2) or ilmenite ($FeTiO_3$) at 1000 °C:

$$TiO_2 \ ; \ FeO \cdot TiO_3 + Cl_2 \longrightarrow TiCl_4 \tag{5.1}$$

$$TiCl_4 + 2Mg \longrightarrow Ti + 2MgCl_2 \tag{5.2}$$

$TiCl_4$ reacts with liquid magnesium at 800 °C in argon atmosphere to form solid metallic titanium and liquid magnesium chloride. This reduction step is a batch process performed at high temperature, the result is the formation of the so called titanium sponge, which is a mixture of magnesium chloride salts and metallic titanium. The chlorides can be removed by acid leaching or via vacuum distillation at high temperature, causing the chlorides to volatilize. If extreme purity is necessary, the sponge can be electro-refined. In the so called Hunter process, sodium replaces magnesium.

This sponge is the raw material for Ti-alloys: the sponge is crushed and alloying elements are added in powder form. After a mechanical blending process (i.e. in a twin cone blender), briquettes are shaped (i.e. using a hydraulic press) and welded together to form the first melt electrode: the melting step is the crucial one to obtain high quality cp titanium or Ti-alloys. In fact, the sponge has very high surface area and, even after vacuum distillation, chlorides or other compounds are still adsorbed to the surface.

Because of the high gas production during the first melt, vacuum arc melting furnace with large capacity pumping system is needed. The arc is started between the electrode and some Ti in the bottom of the copper crucible: Ti drains from the electrode and forms the primary melt ingot. For structural applications the primary ingot undergoes a special step, vacuum arc remelting (VAR), to increase

homogenization and minimize short-range segregation. For very special applications, the ingot can be remelted twice and the product is a triple melt quality grade material (i.e. rotors, moving parts of jet engines). To favour diffusional homogenization, an annealing step about 10 hours in high temperature furnace is performed.

Unfortunately, two different types of melt defects may occur, and even if they are rarely present in Ti-alloys, they can affect seriously mechanical properties.

The first of them is the presence of nitrogen or interstitial elements, the so called Hard Alpha defect. This elements can form stable and high melting compound (i.e. TiN, titanium nitride), very hard and extremely brittle. Fatigue life of highly stressed components with such defects seriously decreases because such hard and brittle particles leads to early crack initiation and propagation.

The second type of defect is known as Soft Alpha, and is the result of chemical composition variations, such as aluminium rich regions. They are dangerous because they leads to the formation of α'' precipitates.

Moreover, there is another general kind of defect, typical of solidification processes: segregation of β-stabilizing elements may occur during ingots solidification. These β-stabilizers rich regions cause a local decreasing of the β-transus temperature, leading to the formation of α-phase poor regions, known as "beta flecks". They have bad effects on the material mechanical behaviour, but not so much as the previous defects.

At the end of the production process, appropriate non-destructive testing method must be carried out to confirm the raw material quality before sending it to a manufacturer/forger, i.e. ultrasonic inspection.

As mentioned before, the high cost of Ti is mainly due to its expensive productive process, as well as absorbing the majority of the world production of magnesium metal and the necessity to operate under inert atmosphere or high vacuum. Much research is currently being made in this field to develop new and cheaper processes: for example, the FFC Cambridge electrochemical process may eventually replace the Kroll one [39].

5.2.2 Processing of Titanium alloys

The microstructure of Ti-alloys can be varied and controlled by selecting the suitable thermomechanical processing: main purpose is to control phase distribution and grain size to the preferred level, in order to achieve the desired properties.

Cp titanium is usually processed in the α field, being subjected to homogenization process, deformation process and recrystallization process (Figure 15). Low temperature deformation (200-300 °C) and even cold deformation (room temperature) is possible, but is important to remember that the formability is decreasing with increasing the oxygen content, from Grade 1 to Grade 4.

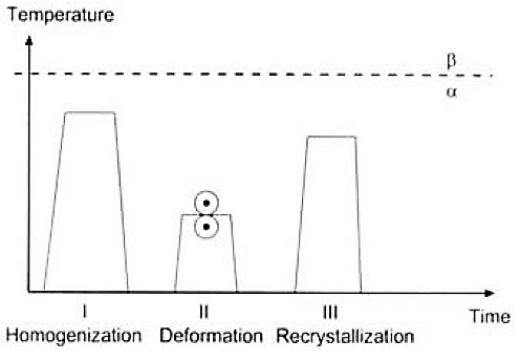

Figure 15: Schematic processing route for cp titanium [36].

The α+β alloys may exhibit three different types of microstructures: fully lamellar structure, fully equiaxed structure and bi-modal microstructure (or duplex).

Bi-modal structure is essentially composed of equiaxed primary α grains in a lamellar α+β matrix. The process is divided into four different steps (Figure 16): homogenization in the β phase field, deformation and recrystallization in the α+b phase field and aging at lower temperature. For each step, there are critical parameters, such us cooling rate for homogenization step, deformation degree and mode for deformation step, temperature, time and cooling rate for recrystallization step, and temperature for aging step.

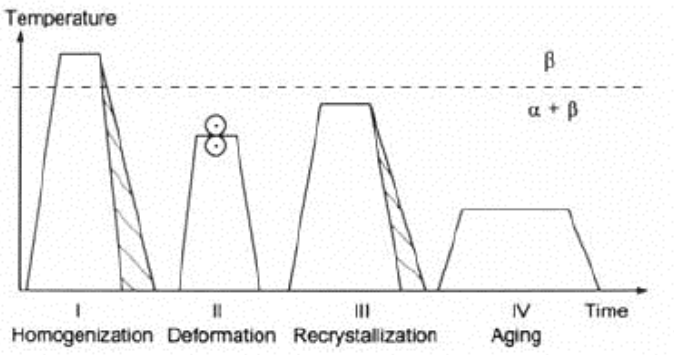

Figure 16: Schematic processing route for bi-modal structure [36].

The cooling rate in step I determines the width of α-lamellae in the lamellar structure; the deformation temperature in step II determines the texture type, the deformation degree varies the texture intensity; the temperature in step III determines the volume fraction of recrystallized α particles located at the triple-points of β grains.

Fully equiaxed structure can be obtained if the cooling rate in the recrystallization step is sufficiently low: the result is the growth of globular α grains, with β grains located at the triple points of α grains.

For fully lamellar microstructure (Figure 17), a homogenization step in the β-phase field is applied after the deformation step, and the cooling rate from homogenization temperature is the crucial aspect of the treatment, because it determines the lamellar structure parameters, such as α lamellae size , α colony size and extension of α layer at β grain boundaries.

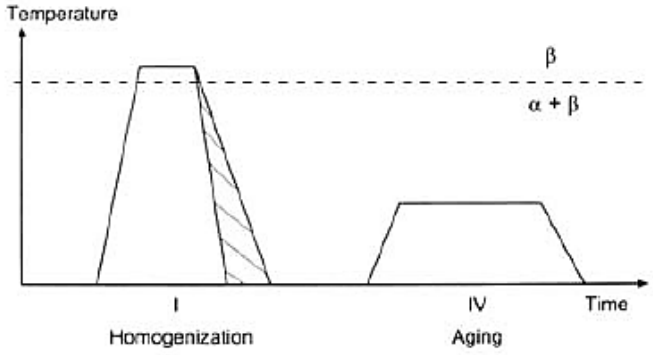

Figure 17: Processing route for fully lamellar microstructure [36].

In β alloys does not occur any martensitic transformation and the β phase can be retained in a metastable form at room temperature if the β-stabilizing elements content is high enough. Figure 18 explains the typical processing route for β alloys.

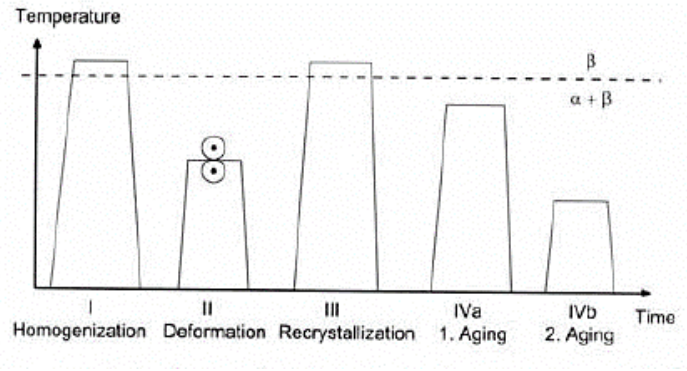

Figure 18: Typical processing route for lamellar microstructure of β Ti alloys [36].

The recrystallization step is performed in the β-phase field, and often a two-step aging is performed. The presence of ω and β' precipitates is to avoid in β-alloys microstructure, but their coherence with the matrix is useful as precursors, favouring a homogeneous distribution of α plates.

Bi-modal structure can be obtained following the process in Figure 19: the heating temperature during recrystallization step is below the β-phase, and round equiaxed α particles are formed, limiting grain growth of β phase during recrystallization.

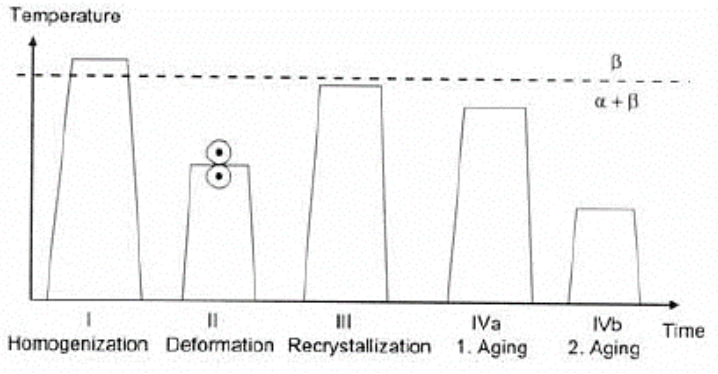

Figure 19: Schematic processing route for bi-modal structure of β Ti-alloys [36].

Necklace microstructure comes from the "through-transus" deformation process: after homogenization, the material is directly deformed from β phase field through

α+β phase field, inducing α phase to form at the deformed β grain boundaries. Processing parameters are difficult to control, and it is important that the deformation process is completed before α particles start to precipitate as round particles.
The final microstructure is formed by short segments of α-layers at deformed β grain boundaries.

5.2.3 Factors affecting properties of Ti alloys

Thus, microstructures of titanium can be complex, and here were discussed only main features without being exhaustive. Microstructures depends on many factors, such as composition, processing and post processing heat treatments. Varying of alloying elements and thermomechanical processing techniques can develop to a wide range of properties assumed by Ti alloys.
Properties of particular interest in structural orthopaedic applications are the following:

- UTS and YS
- Ductility
- Toughness
- Fatigue properties
- Crack propagation in fatigue or under environmental constraints

Each of these properties can be affected by one the mentioned factors, or by a combination of them; such as alloying elements and impurities, type of melting process and melting steps, number of forging steps, surface treatments,…
Cold machining or working is not always possible, because titanium tends to seize and very sharp tools with slow speed are required. Another difficulty in cold forming titanium is the occurrence of the springback, due to the relatively low modulus and high yield stress. Then most care is taken during machining, because tolerances for diameters, roundness, straightness and angles are very tight in prosthetic applications (and usually where the use of Ti is essential). Dimensional inspection may be checked under microscope or carried out on a multi-axis measuring machine.

Welding, if required, must be done in an inert atmosphere of argon or helium to shield the material from contamination with atmospheric gases such us O, N or H, because these elements provoke embrittlement.
Thus, by controlling and manipulating phases properties and grains properties, such as phase distribution, grain size and shape or boundary arrangements, it is possible to control and design final product properties with high precision, in order to reach the best performance in the desired application.
The success of Ti alloys in orthopaedic applications is to be found especially in its specific strength, higher than any other implant materials, and in its excellent corrosion resistance.

5.3 Titanium alloys for orthopaedic applications

Hard tissue replacement is the typical application of metals as biomaterials, and titanium is the most diffusely used, for long bone repairs, joint replacements and dental implants. Ti6Al4V has approximately the same fatigue strength of CoCr alloys, with half of the density than CoCr alloys and better corrosion resistance [40].
Although Ti is a very reactive element, his corrosion stability is due to the layer of formula $Ti_{1+\delta}O_2$ on its surface, capable to passivate the bulk metal: the thickness of an air-formed passive layer is less than 20 nm. It is effective in oxidizing environments, such as salt solutions or acid solutions; but it isn't effective in reducing conditions or in presence of fluoride ions. Due to its oxide layer's high biocompatibility and non-toxicity, Ti is a bioinert material with the special ability to osseointegrate, which is the main purpose for dental and orthopaedic implants.
It has also lower modulus of elasticity than SS or CoCr alloys, so the bones can share more load and avoid degradation, caused by the lack of stress and the consequently decrease of the bone section and the release of calcium, till a new equilibrium is achieved, how it is assumed by the Wolff's law.
The bone is a living tissue constantly evolving during time, while the implant has to guarantee his performance for many years: because of this, devices with mechanical properties several times greater than those of bone are required. Fatigue strength and

elastic modulus of the most used biomaterials for orthopaedic applications are compared with those of bone in Table 7.

Table 7: Mechanical properties of different biomaterials vs. cortical bone properties [16].

	Fatigue Strength σ_f [MPa]	**Elastic modulus E [GPa]**
Bone	30	22
Metals		
FeCrNiMo (316L)	250	210
CoCr, cast	300	200
CoNiCr, wrought	500	220
Ti alloys (α+β)	550	105
cp Ti	200	100
cp Nb	150	120
cp Ta	200	200
Ceramics		
Al_2O_3	0-400	380
ZrO_2	0-450	170
Polymers		
PMMA	30	25
UHMWPE	16	1-2

5.3.1 Bone-implant interaction

Chemical and mechanical interaction between bone and implant is the most important aspect to take care since the two are combined into a new composite structure: unlike other metals, Ti does not induce formation of fibrous tissue barrier when placed in contact with healthy bone [37]. This is a great advantage because it allows bone to grow on the implant surface.

The surface structure of an implant has a significant influence on both its anchorage and its strength of adhesion to the tissue. Measurable adhesion strength to the bone is present only with a minimum of surface roughness, which allows new bone particles to adhere resulting in a better linkage.

Besides the favourable influence on the implant anchorage, there is a further important advantage of surface structuring: the improvement of load transfer encourages the health of the bone, avoiding decalcification or soft tissue to growth.

Therefore, the effect of a much stiffer bone implant is to reduce the loading on bone, resulting in the so-called "stress shielding" phenomenon. Because of this, high difference between the Young's modulus from the implant to the bone should be avoided; by comparison, gradual transition in Young's modulus or even isoelastic behaviour helps to avoid delamination stresses at the interface and provides the stimulation of new bone formation (Figure 20) [16].

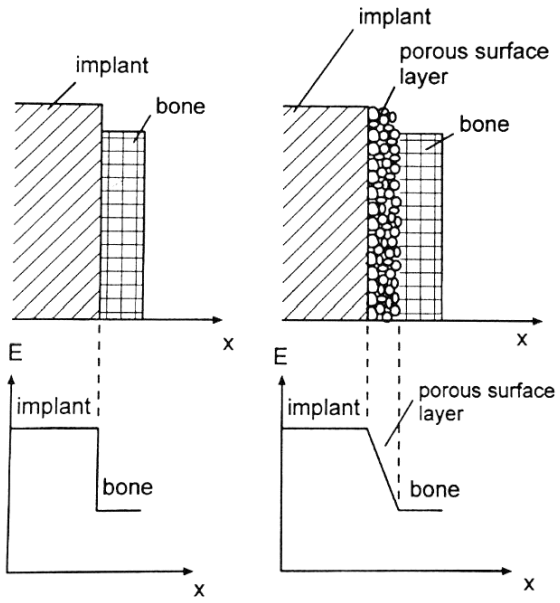

Figure 20: Change in Young's modulus at bone implant interface with smooth and porous surface (schematic) [16]

Thanks to Ti alloys suitable Young's modulus value, it is possible to design with porous coated titanium a tailored stiffness in the surface layer (controlling coating thickness and coating porosity), producing an engineered material, which gradually reduces the difference in elastic behaviour and promotes an appropriate ingrowth of bone in the intentionally introduced pores.

The elastic modulus of a porous material might be approximated by equation:

$$E_p \approx E_0 \, (\, 1 - a \cdot \phi^b \,) \tag{5.3}$$

Where E_p is the elastic modulus of the porous material [GPa]; E_0 is elastic modulus of the non-porous bulk material [GPa], p is the porosity and *a, b* are constants.

Consequently, density of a porous material changes according to:

$$\rho_p \approx \rho_0 \, (\, 1 - \phi \,) \tag{5.4}$$

With a porosity of 30%, the Young's modulus of titanium becomes closer to that of bone (Figure 21), which lies between 15 and 30 GPa [41].

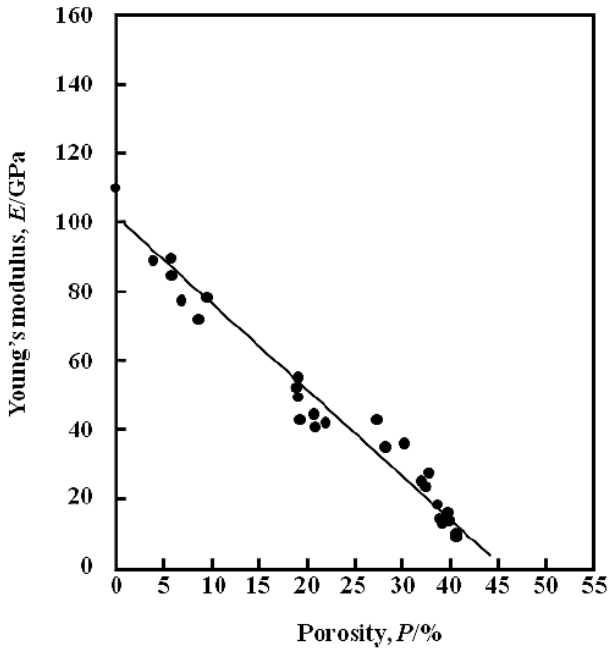

Figure 21: Dependence of porosity on apparent Young's modulus of porous titanium [41].

By this, the stress shielding effect, induced by the non-homogeneous load transfer between the bone and the implant, decreases, preventing the implant to loosen or the bone to re-fracture.

However, as mentioned above, Ti and its alloys are known to have a certain amount of notch sensitivity, which decreases fatigue behaviour. The fatigue strength of porous-coated alloys is inferior to that of uncoated wrought or forged materials, and stress raisers induced by porous coating or non-uniform bone ingrowth may cause these implants to break and fail.

Furthermore, because of titanium low shearing resistance, implants should be provided with a wear-resistant coating, such as oxides and oxynitrides, carbides and carbo-nitrides or nitrides of transition metals. Another option to improve implant lifetime is to coat it with a bioactive material (such as "Bioglass"), suitable to favour adhesion and new bone formation. An ideal bioactive coating would bond tightly

both to the bone and to the implant, and this reduce the choice on the materials able to be coupled: for instance, metals can be hardly coated by ceramics, because high thermal stresses are generated during processing of materials with such a difference in thermal expansion coefficient. Moreover, chemical reactions between the ceramic and the metal can weaken the metal interface, and Ti is a very reactive material with oxide materials. Several method for surface modification are available (CVD, PVD, plasma spray, etc.) and their effect on the prosthesis performance has to be evaluated carefully, such as the introduction of residual thermal stresses and stress raisers or the unexpected influence on other properties (fatigue strength, corrosion resistance, etc.).

One problem may raise with low-modulus materials such as Ti alloys, and it is the springback effect. However, recent developments of new low-modulus Ti alloys (such as Ti12Cr or Ti30Zr5Mo) with the capability of the so-called "self-adjustment" of the modulus, can lead to perfectly designed implant materials. The modulus self-adjustment performs in certain β-type Ti alloys in response to the appearance of deformation-induced phases such as α', α'' or ω. Specifically, the modulus decreases in region with deformation-induced α' and α'' phase, and it increases with the presence of deformation-induced ω-phase. In case of ω-phase formation, the deformed part will have high modulus with low tendency to springback. Thus, elastic properties of the implant can be further tailored to the need of surgery and biomechanics [42].

In conclusion, Ti-base alloys seem to fulfil all mechanical, clinical and biological requirements, resulting to be one of the best biomaterial today available for orthopaedic applications and prosthesis design.

As in this work mechanical behaviour of porous coated Ti samples is simulated and tested, the evaluation of the "in vitro" response is the basis from which investigate on further developments. The main purpose of porous coated prosthetic devices is to favour the osseointegration, providing a more benign stress condition at the bone-implant interface and allowing fluids to flow inside them, promoting bone healthy growth. With porous coated devices, problems may raise from wear particles produced by abrasion and the accumulation of metal wear particles in periprosthetic

tissues can lead to metallosis and osteolysis. Obviously, number and type of metal particles cannot be estimated precisely as these factors depend on the type of alloy, design of the prosthesis, the applied forces, the expected duration of the device, etc… These are the main reason why the material response to dynamic mechanical loads has to be accurately studied, in order to prevent any premature, highly undesirable failure.

6 SIMULATION OF Ti-ALLOY BIOMECHANICAL BEHAVIOUR

As follows from results shown in chapters 2 and 4 , to correctly understand behaviour of the implant material, 3D analysis has to be carried out. It is very difficult, if not impossible, to measure three-dimensional distribution of strains and stresses in the volume of the specimen and its differences in the porous coated layer. In the case of poroelasticity, this is also complicated by fluid flow, which does not allow any type of contact measurements, since they will disturb the flow itself. Therefore the modelling of materials behaviour is an excellent tool to understand how stresses and strains are distributed, compared with the actual orthopaedic loading conditions.

In this work modelling of biomechanical behaviour was implemented with COMSOL Multiphysics (CMP). It is a finite element analysis (FEA) software for the modelling and simulation of complex physical systems based on partial differential equations (PDEs). Its strong point is the ability to model and simulate multi-physical phenomena combining different modules and linking different variables. When solving the models, CMP may also use adaptive meshing and error control using a variety of numerical solvers [11]. The discretisation of the original problem with a finite number of unknown parameters is the crucial step of FE method, approximating PDEs with algebraic equations. The number of unknown parameters at every nodal mesh point is the number of degrees of freedom (DOF) for the considered problem, which is an important parameter for estimation of computational time and cost. In this work, Structural Mechanics module of CMP is used to describe the material dynamic mechanical behaviour.

6.1 Modelling conditions

The goal of the simulation is to build a model able to reproduce the material response to dynamic forces, such as those happening during normal human activities.

As the titanium specimen used in prosthesis design is coated by a porous titanium layer to help osseointegration, the consequences of the presence of the porous layer in the mechanical response are one the main interests of the work. The porous coating create a non-homogenous structure, whose in vitro behaviour must be studied before its application in the body. Such conditions are rather complex themselves, here a simplified three-point bending mode is considered, as it is easily realizable in the DMA testing environment. However, standard DMA does not have a theory for a simple estimation of e.g. elastic modulus or other dynamic parameter for non-homogeneous specimens and therefore only modelling would give more consistent picture.

During three-point bending test, the material is bent under the action of a vertical force while sample is resting on the two lateral supports: Figure 22 schematically shows the generated stresses state concept (exaggerated).

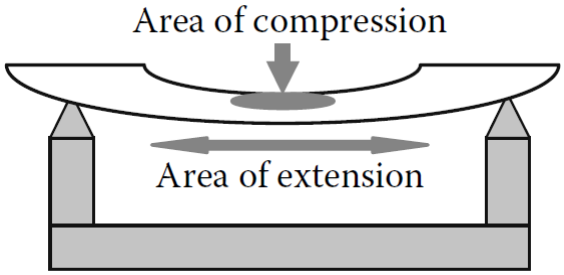

Figure 22: Stresses generated in 3-point bending [5].

The specimen geometry is limited by the constraints of the equipment: the length (along the x-axis) is fixed at 15 mm, width (y-axis) is equal to 3 mm with a distance between supports of 10 mm (Figure 23).

Considering the symmetrical shape of the specimens, two planes of symmetry exist: surface 1 lies in the y-z plane of symmetry and surface 2 lies in the x-z plane of symmetry. Therefore, only ½ or ¼ of the specimen needs to be simulated as the stress state and deformations will be mirrored into the other parts.

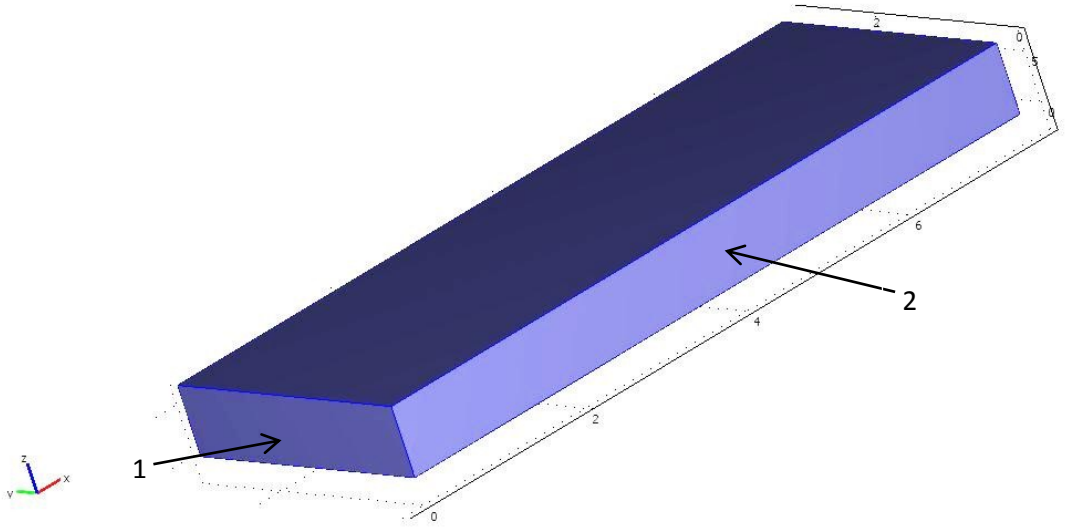

Figure 23: Sample geometry

As the specimens simply rest on the equipment supports, the constraint of zero displacement along the z-axis is applied on the edge representing the support itself (Figure 24) Here the support is considered as a rigid roller, because the deformation of the support in DMA is measured separately and automatically subtracted to record the deformation of the specimen alone.

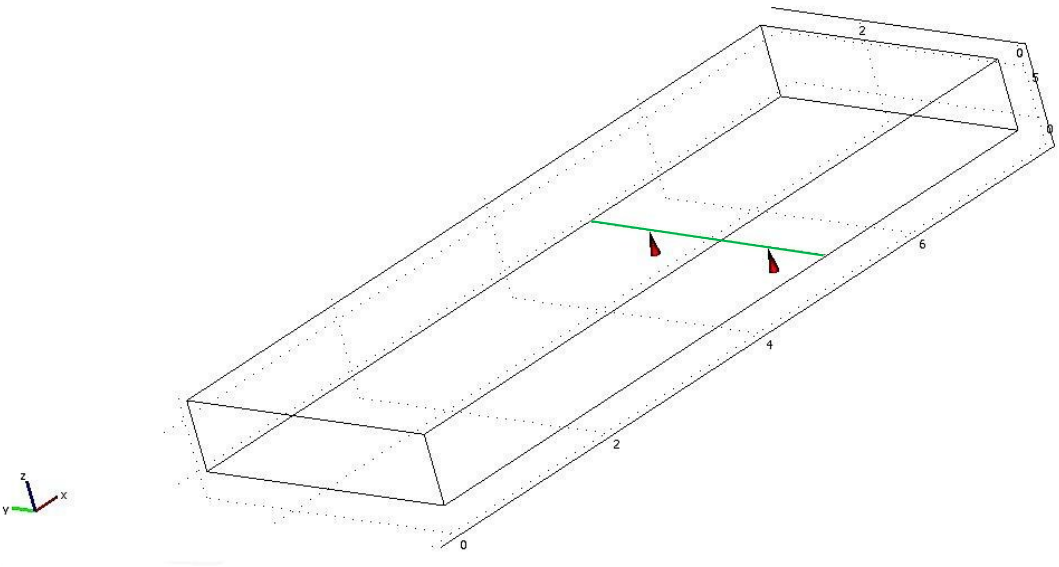

Figure 24: No z-displacement is allowed for elements laying on the support, represented by the green line and the triangular marks oriented along the z-axis

In this work, three main variables have been used for input, namely the thickness of the specimen, the thickness of the coating layer (including zero for non-coated

materials) and the porosity of the coating. Different values of samples' thickness (z-axis) were studied, and both bulk and porous coated specimens were simulated.

For the study of the elastic response of the specimens and keep it within the theory of thin plates bending (small deformation), the obtained maximum relative displacement must be less than a reasonable value, i.e. < 0.05 (5%) of the total thickness of the specimen.

The specimen is bent under the application of a force F_{load} acting along the y-z plane intersecting the medium section of the sample (Figure 25). This force is the result of the algebraic sum of a static force (constant value during time) and a dynamic force.

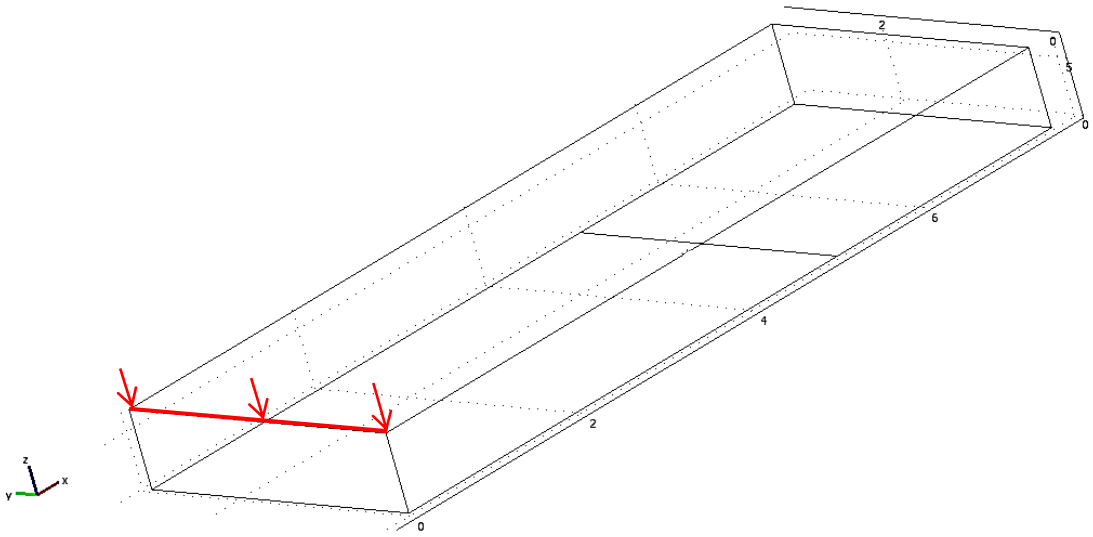

Figure 25: F_{load} direction and application.

The dynamic force oscillates with a frequency value f between the range $\pm F_{dyn}$, following a sinusoidal wave:

$$F(t) = F_{dyn} \cdot \sin(2\pi \cdot f \cdot t) \tag{6.1}$$

while the static force, necessarily bigger than the dynamic one, keeps the sample always slightly bent in the –z direction. Thus, the resulting applied force F_{load} is expressed by:

$$F_{load} = F_{stat} + F(t) = F_{stat} + F_{dyn} \cdot \sin(2\pi f t) \tag{6.2}$$

As the frequency value is set equal to 1 Hz, the maximum force is applied at the time 0.25 of each loading cycle (Figure 26).

The ratio of F_{stat} on F_{dyn} is the proportional factor, PF. In our simulations, the proportional factor varies in the range $1.2 - 1.4$.

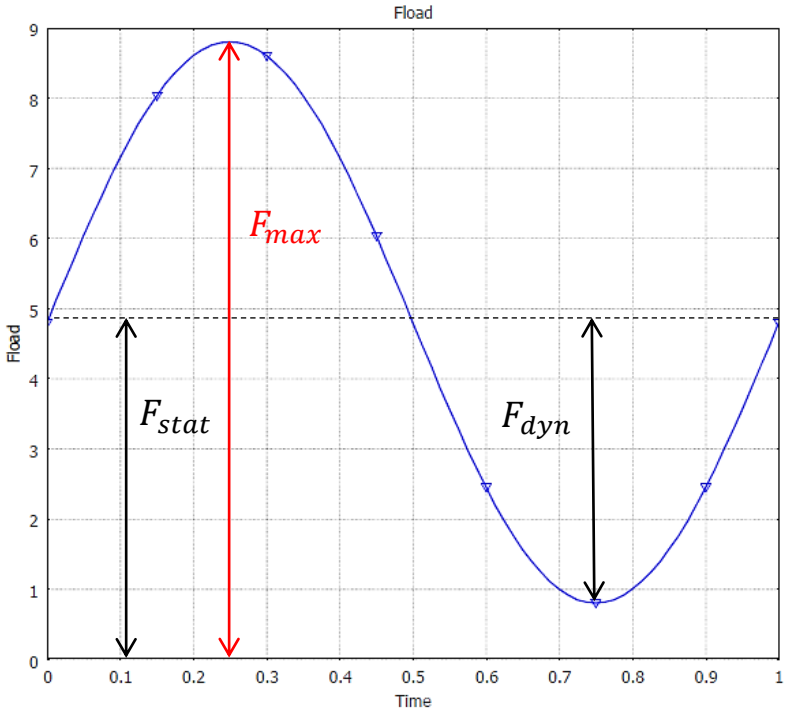

Figure 26: Example of force applied by the pushrod on the specimen; F_{dyn} = 4 N, PF = 1.2

Moreover, another force is always acting on the specimen, and it is the pre-bending force, which guarantees an offset displacement of about 10 µm, required by the instrument. As these data are not recorded during the measurements, a non-zero initial bending force is applied to pre-bend the specimen down to ~10 µm, which has to be implemented into the model.

Ti-alloys properties (mechanical, thermal, electrical,…) values were taken from the built-in CMP's Material Library, but they can be tailored according to the needs. For instance, Young's modulus of bulk titanium is set equal to 100 GPa, and the density equal to 4.6 g·cm^{-3}. However, the same properties for a porous titanium sample need to be calculated, and it can be done automatically by introducing equations (5.3) and (5.4) in CMP.

The discretisation step is automatically performed by the meshing tool of CMP: in Figure 27 the default free-mesh parameters are used, with one refining step .

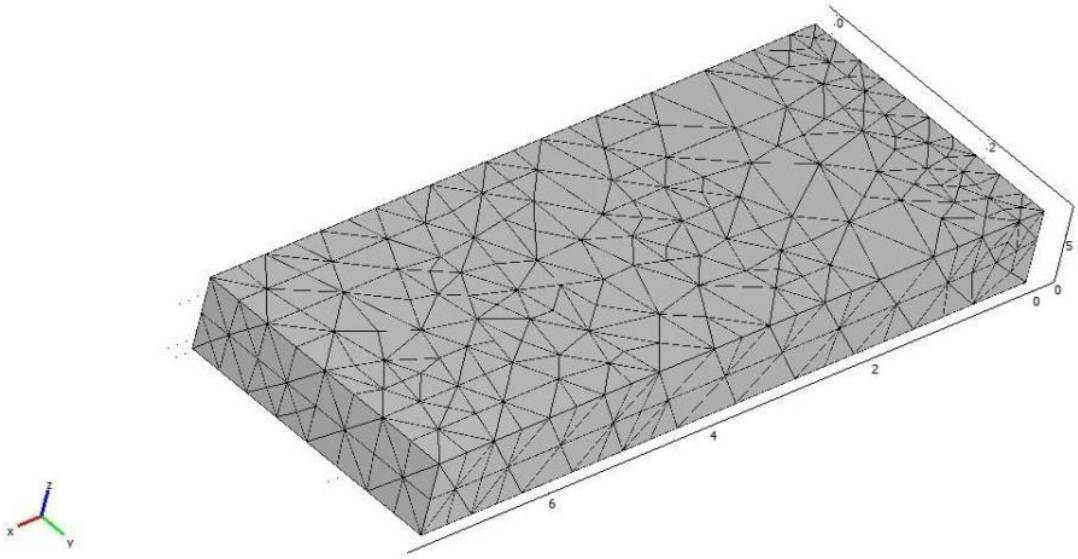

Figure 27: Mesh visualization

The solving step involves a time dependent transient analysis, with a chosen time stepping value of 0.0125 s: for an every second, which corresponds to a complete loading cycle of 1 Hz, eighty solutions are calculated and stored.
The investigated output data were the values of the absolute displacement and the relative strain: from them is possible to calculate the time dependent Young's modulus, which is one the DMA equipment output data used to correlate the simulation results with the experimental results.

6.2 Experimental conditions

Examined samples' thickness adopted in this study were in the range 0.6 – 1.2 mm. For greater thickness, the force required to reach the minimum displacement exceeded the maximum force applicable by the pushrod; on the other hand, for thickness less than 0.6 mm, the resulting strain was higher than the fixed limit of 5%, even with very little applied force. Besides samples' thickness, other parameters involved in these simulations are the coating thickness, coating porosity, and applied

dynamic force/static force. To check the validity of the results from CMP, three-point bending tests were performed with Netzsch DMA 242 C (Figure 28).

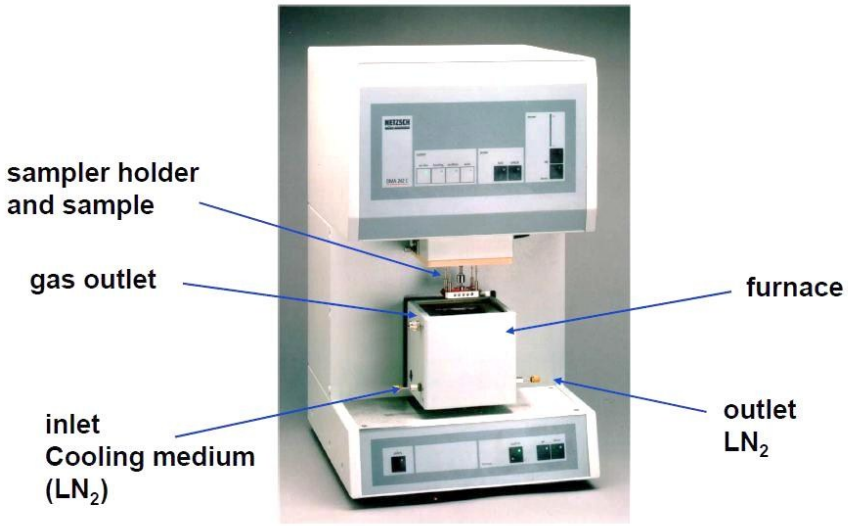

Figure 28: Netzsch DMA 242 C [43].

A schematic description of the equipment is given in Figure 29. The apparatus is able to perform temperature-time studies (fixed frequency), frequency studies (fixed temperature) or dynamic stress-strain curves (dynamic force changing at a fixed rate).

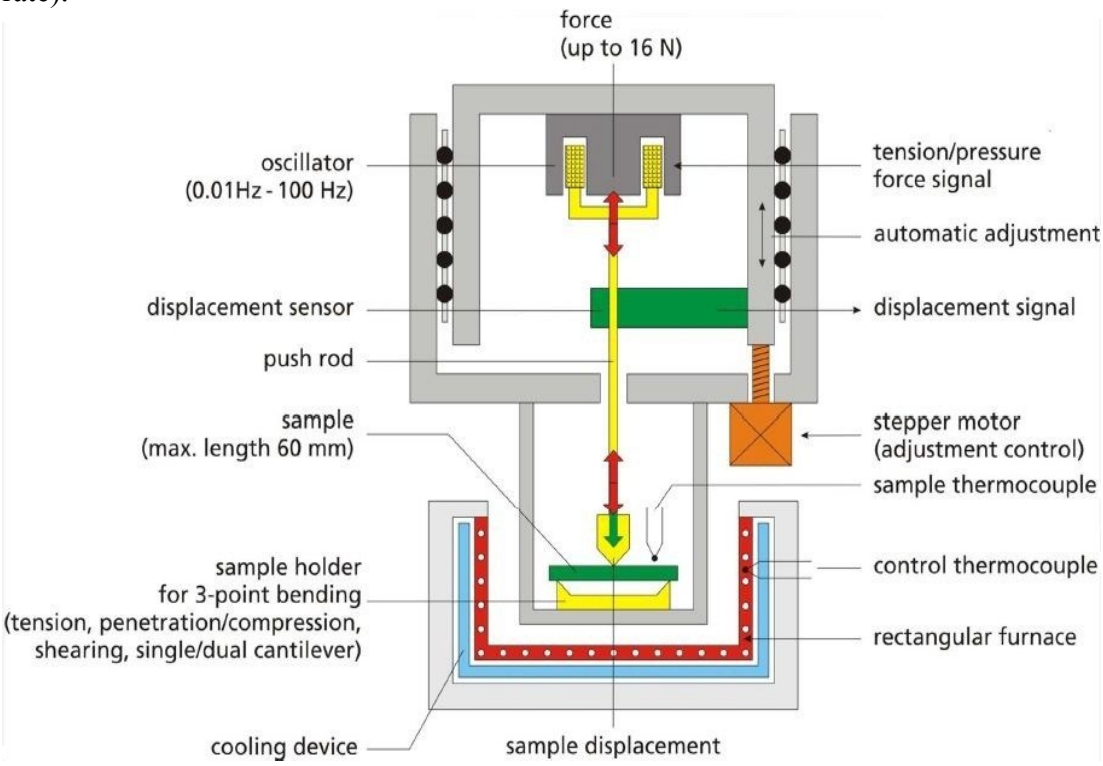

Figure 29: Schematic description of the Netzsch DMA 242 C [43].

The apparatus was equipped with the 3-point bending fixture, with a length of 50 mm and a maximum specimens capacity of 60 mm for length and 5 mm for thickness. The maximum force applicable by the push rod is equal to 16 N. Tests were performed at room temperature, without the use of the furnace (i.e. at room temperature).

The instrument requires at the input the dimensions of each samples, from which it can calculate the correct geometric factors to determine the real stresses and the amount of deformation of the samples. The dimensions for rectangular shape are width (x), height (y) and depth (z), and for the three-point bending fixture the geometric factor is:

$$GF = \frac{x^3}{4zy^3} \tag{6.3}$$

while the time-dependent modulus is correlated to the displacement a^* by:

$$E^* = \frac{F^* \cdot GF}{a^*} \tag{6.4}$$

Since thickness involved in these equations is cubed, small errors in dimensions can generate large errors in module measurement, even in the linear region.

Inertia effect and shear heating are other problems affecting these type of measurements, when carried out at high frequencies. However, with the frequency value fixed at 1 Hz these effects can be neglected.

The Netzsch DMA 242 C, through the installation of a special sample holder (Figure 30), can perform also measurements with specimens immersed in liquid environment: this features will be exploited in the future to investigate the poroelastic behaviour of porous coated samples.

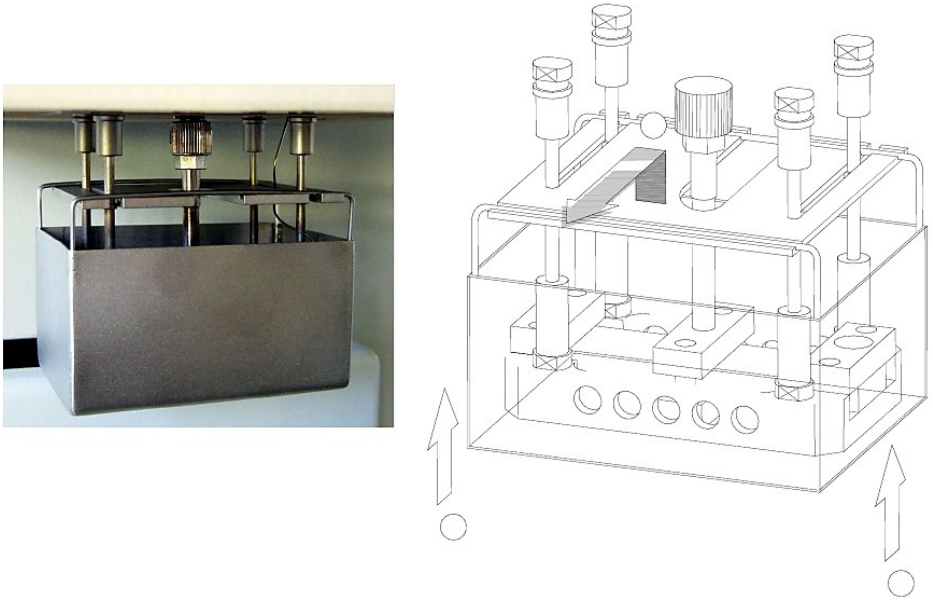

Figure 30: Sample holder for measurements in liquid environment [43].

Three-point bending validation tests were performed with aluminium specimens, since titanium coated specimens were not yet available at this moment with required tolerances. To simulate coating as a material layer with lower modulus, plastic (polypropylene) specimens were additionally applied and aluminium + thick plastic composite specimens have been specially prepared. Each of the previous specimens exhibited different dimension characteristics and, of course, a range of mechanical properties.

The maximum displacement (amplitude) achievable by the push rod was limited in the range ± 50 µm from the zero offset position, namely when the dynamic force is zero and only the pre-bending force and the static force are acting on the sample.

7 RESULTS AND DISCUSSION

7.1 Modelling results for titanium specimens

The results of modelling with COMSOL Multiphysics are visualized in a graphical form first during post-processing of the data. For example, Figure 31 (next page) shows the specimens z-displacement at the time 0.25 seconds (= ¼ of the oscillation cycle), when the maximum bending force is acting on the sample. In this example, one can see that the maximum deflection of the specimen in the centre reaches -17.8 µm, and the displacement of the free edge of the specimen is +13 µm.

Table 8 shows results from COMSOL simulations on uncoated titanium specimens, for different thicknesses, from 0.6 mm up to 1.2 mm. Acting force and proportional factors vary in order to reach a minimum of about ~10 µm, but not to exceed the maximum allowed deformation limit.

Table 8: Simulation results for titanium specimens without coating

Total thickness [mm]	**PF**	**F_{dyn} [N]**	**F_{max} [N]**	**Max Relative displacement [%]**	**Max Absolute displacement [µm]**	**Elastic Modulus [GPa]**
0.6	1.2	2	-4.4	2.63	-15.76	107.70
0.7	1.2	2	-4.4	1.47	-10.33	103.39
0.8	1.4	6	-14.4	2.74	-21.91	106.99
0.9	1.4	7	-16.8	2.00	-18.01	106.69
1	1.4	8	-19.2	1.51	-15.08	106.08
1.1	1.4	8	-19.2	1.03	-11.33	106.10
1.2	1.4	8	-19.2	0.73	-8.75	105.76

The elastic modulus of titanium entered at the beginning of simulations was chosen as 100 GPa. However, as seen from the Table 8, there is a difference about 6% between the input and output elastic modulus values.

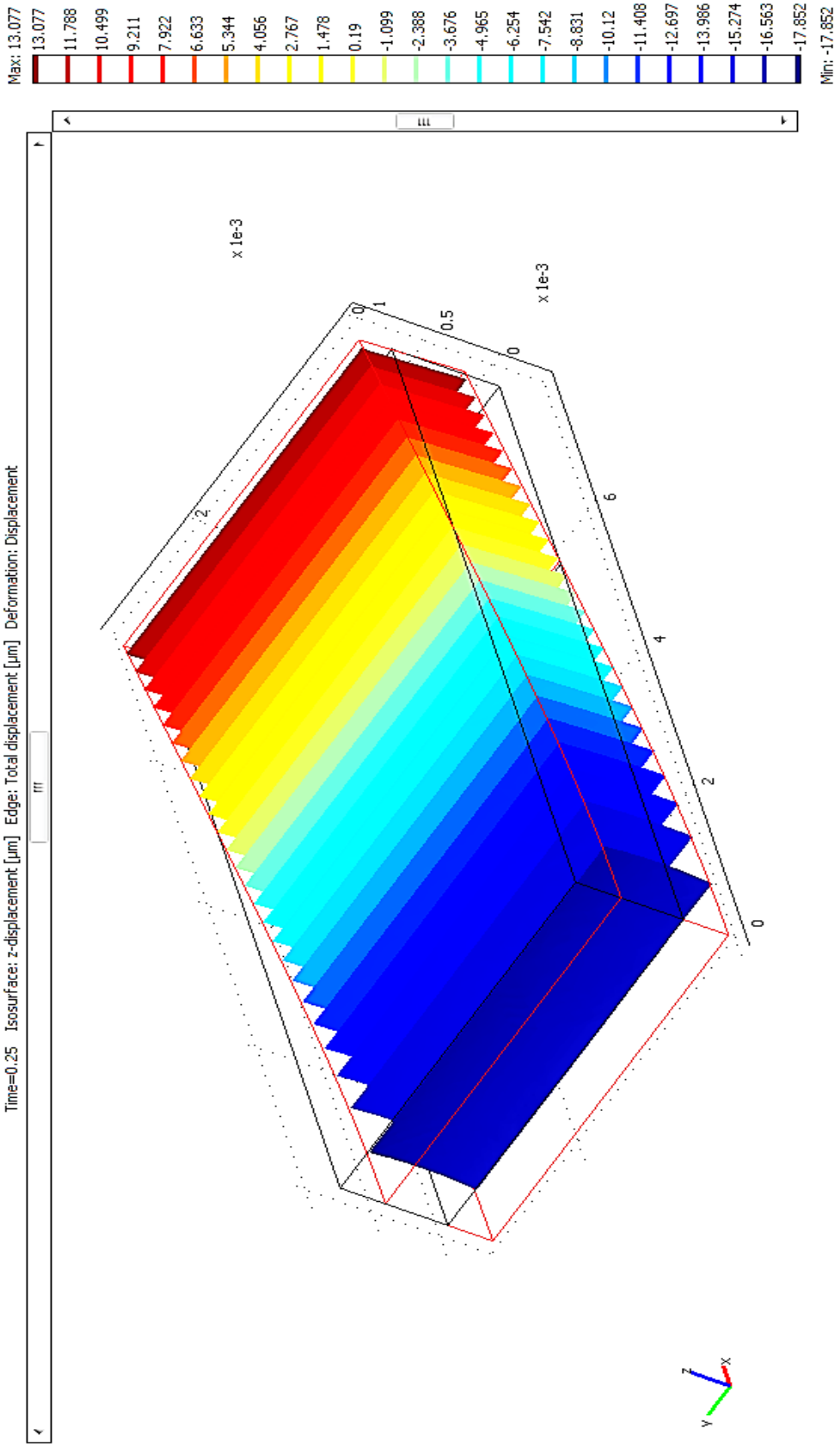

Figure 31: Z-displacement [µm] visualization during post-processing analysis (0.8 mm thickness; 6 N dynamic force, 1.2 PF)

The reason for that is that elastic modulus calculated from the geometric factor and stiffness defined as ratio of the force to the displacement (equation (6.4)), does not include the effect of the Poisson's ratio, which affects the material response:

$$E_{meas} = \frac{E_0}{1 - \nu^2} \tag{7.1}$$

For a Poisson's ratio value of ~0.3, this correction is about 1/0.91, which roughly gives the observed 6-7% increase in the simulated modulus (Table 8).

In order to allow increased thickness of the specimen due to extra coatings and to keep them remaining within the testing parameters limits, it was noticed that the optimal titanium sheet thickness is about 0.7 mm. It does not require high forces to be sufficiently bent and can be coated without the risk of incurring side effects due to the too thin substrate thickness during coating process.

In Table 9 results from simulated tests with porous coated titanium sample are presented: coating thicknesses of 100, 200 and 300 μm on 0.7 mm titanium sheet are considered, with the porosity value varying in the range 20–45 %.

Table 9: Results from porous coated titanium samples

Total thickness [mm]	Coating thickness [μm]	Porosity	PF	Fdyn [N]	Fmax [N]	Absolute Displacement [μm]	Stiffness [N·mm^{-1}]	Elastic Modulus [Gpa]
0.8	100	0.45	1.2	4	8.80	-18.45	476.85	77.61
0.8	100	0.20	1.2	5	11.00	-19.89	553.05	90.02
0.8	100	0.45	1.2	5	11.00	-23.28	472.46	76.90
0.8	100	0.20	1.4	6	14.40	-26.06	552.55	89.93
0.8	100	0.45	1.4	6	14.40	-30.19	477.03	77.64
0.9	200	0.20	1.2	6	13.20	-17.84	739.84	84.57
0.9	200	0.30	1.2	6	13.20	-19.58	674.06	77.05
0.9	200	0.45	1.2	6	13.20	-22.30	591.81	67.65
0.9	200	0.20	1.4	6	14.40	-19.64	733.37	83.83
1.0	300	0.40	1.2	9	19.80	-27.48	720.56	60.05
1.0	300	0.20	1.2	9	19.80	-20.84	950.07	79.17
1.0	300	0.45	1.2	9	19.80	-29.44	672.58	56.05
1.0	300	0.30	1.2	9	19.80	-23.89	828.84	69.07

Figure 32 presents the effect of the coating on the material elastic response: a linear dependence of the time dependent Young's modulus of the coated specimens is evident, according with literature results (Figure 21).

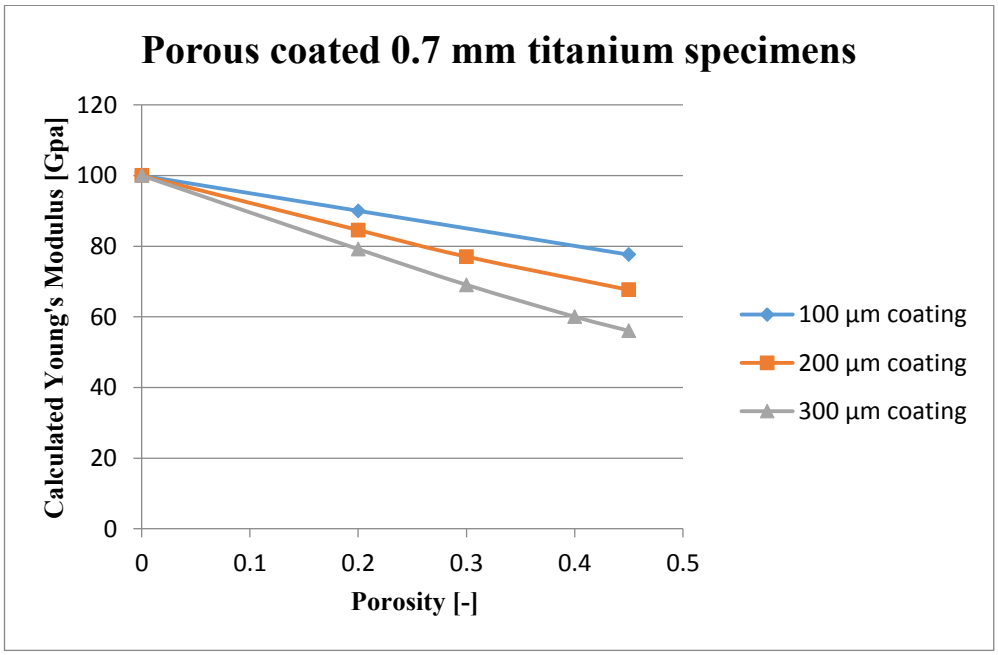

Figure 32: Effect of coatings porosity and thickness on Young's modulus values of porous coated Ti.

The simulated data show that when titanium plate with 0.7 mm thickness is chosen, it would also allow DMA testing of it with extra coatings up to 0.3 mm, if these coatings will have sufficient porosity.

In the following pictures several study cases are presented, showing different properties and behaviours, which can be investigated with post-processing tools available in CMP.

In these pictures, the considered time is 0.25 s (maximum aging force), the selected thickness is 0.7 mm and the dynamic force has a value of 2 N with a PF equal to1.2.

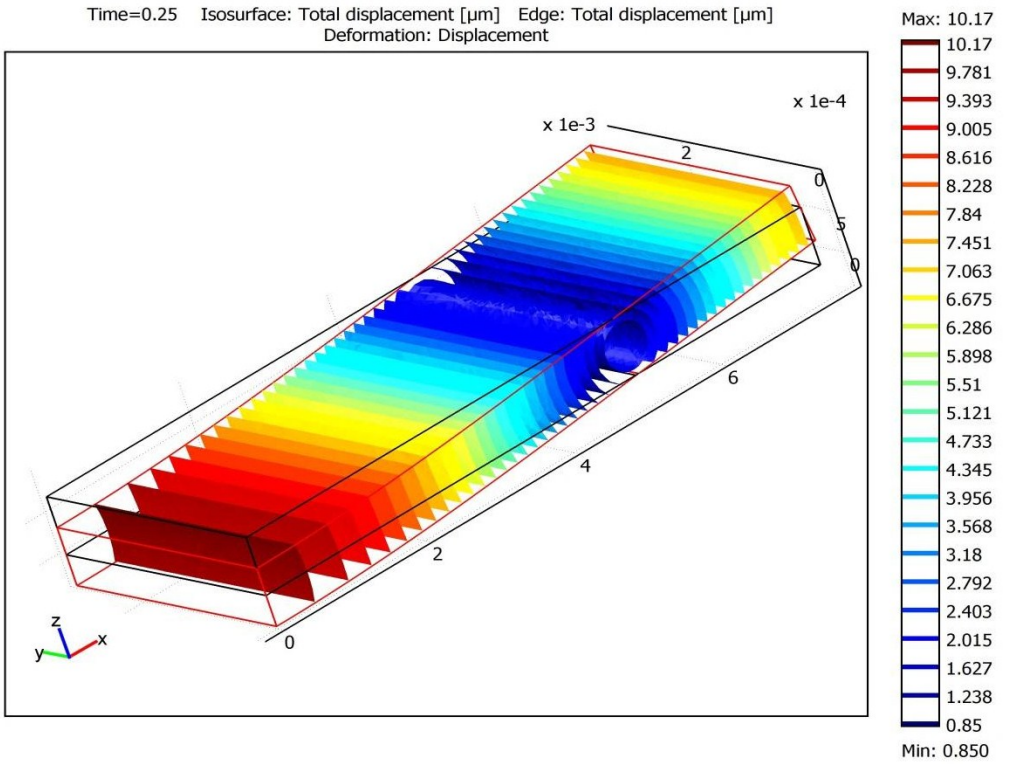

Figure 33: Total displacement [µm]: the elements laying over the support line do not have any displacement, while most of the displacement occurs along the z-axis (Figure 31).

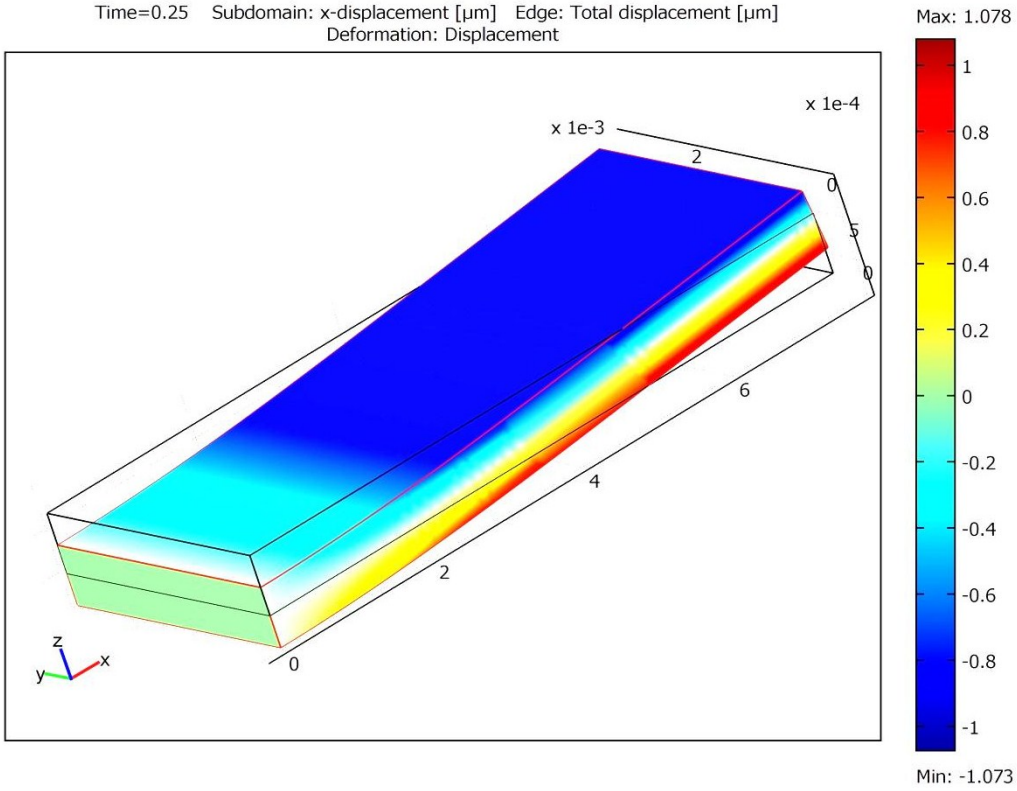

Figure 34: A small (±1 µm) x-displacement occurs in the free edges of the specimen

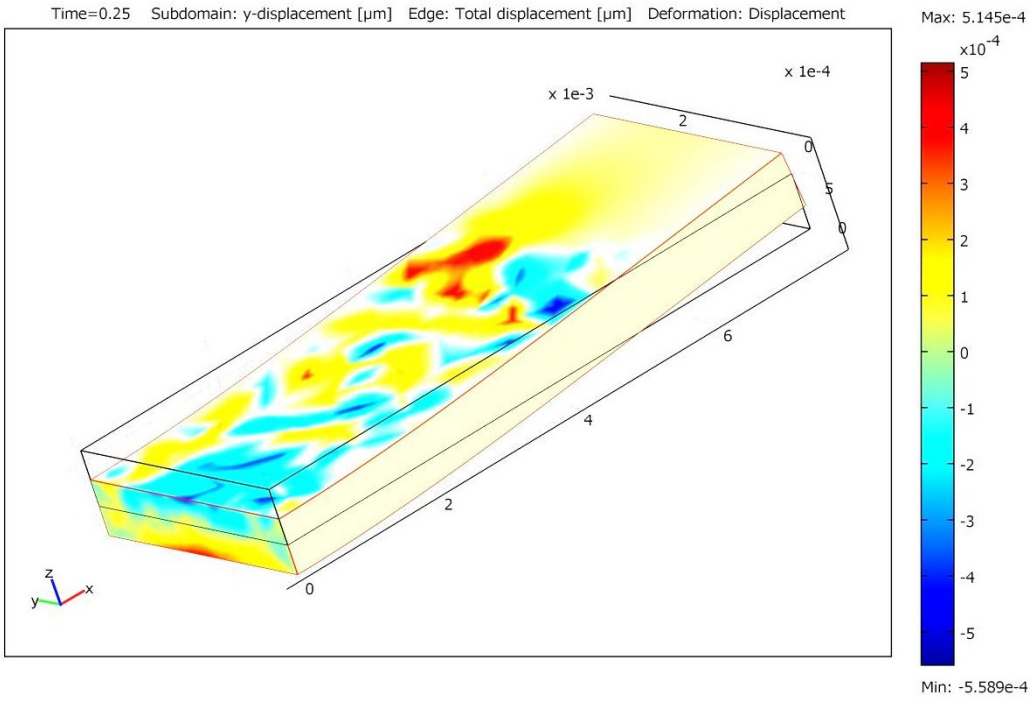

Figure 35: The maximum y-displacement has a calculated value of $5.14 \cdot 10^{-4}$ µm and it has to be considered as zero value due to the symmetry of the problem.

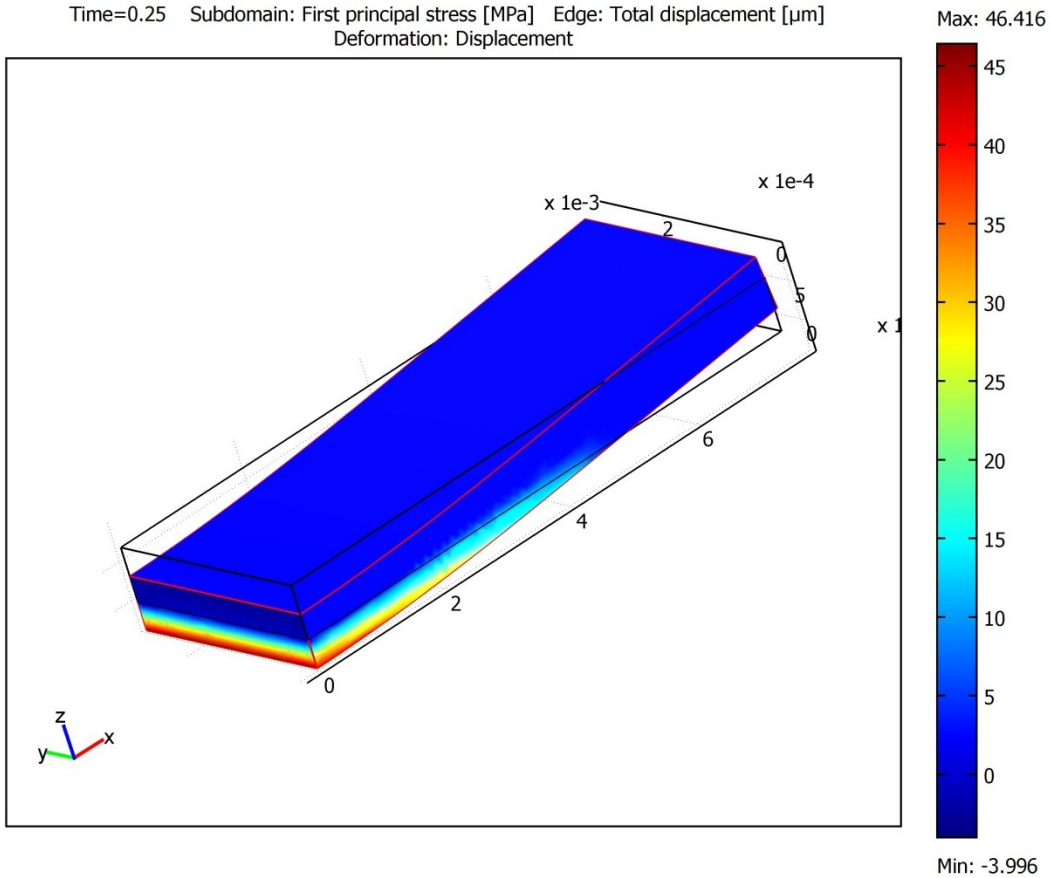

Figure 36: First principal stress [MPa], highlighting the tensile stress of 46.4 MPa in the lower face of the specimen.

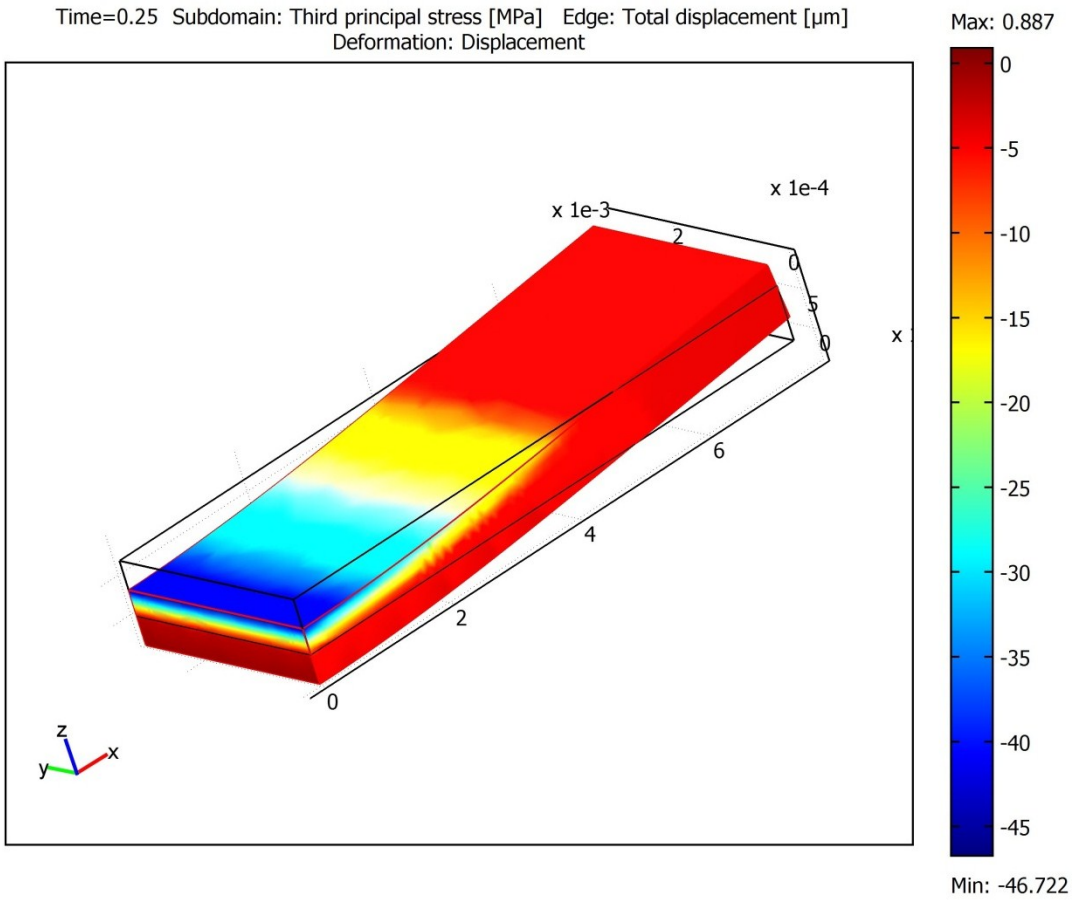

Figure 37: Third principal stress [MPa], highlighting the compressive stress of 46.7 MPa in the upper face of the specimen

7.2 Model Validation

The materials tested with the lab equipment were reproduced with CMP three-point bending simulated tests: the purpose of the validation is to verify if the model can reproduce the experimental results with good accuracy. Materials dimensions and mechanical properties are part of the constants required by the model, and the desired output data is the value of the displacement (Table 10) at a given time and the corresponding value of the Young's modulus (Table 11). An example is reported in Figure 38 (next page), showing that the maximum displacement of the simulated plastic specimen along the z-direction is equal to 112 µm.

Table 10: Experimental and simulated displacement values under the action of F_{max}

Material	DMA displacement a [µm]	COMSOL displacement a [µm]	Corrected COMSOL displacement a [µm]	Δa [%]
Aluminium	99.96	112.35	102.35	2.01
Plastic	98.95	113.47	103.47	4.36
Al+plastic	99.84	108.86	98.86	0.90

Table 11: Experimental and simulated values of the Young's modulus

Material	DMA Modulus E [GPa]	COMSOL Modulus E [GPa]	ΔE [%]
Aluminium	68.53	66.68	1.82
Plastic	1.46	1.45	0.68
Al+plastic	5.63	5.68	0.89

The difference between experimental and simulated displacement values can be attributed to the effect of the pre-bending force applied by the instrument: this force, the value of which is not recorded, has to guarantee a little displacement of about 10 ± 2 µm before the test begins.

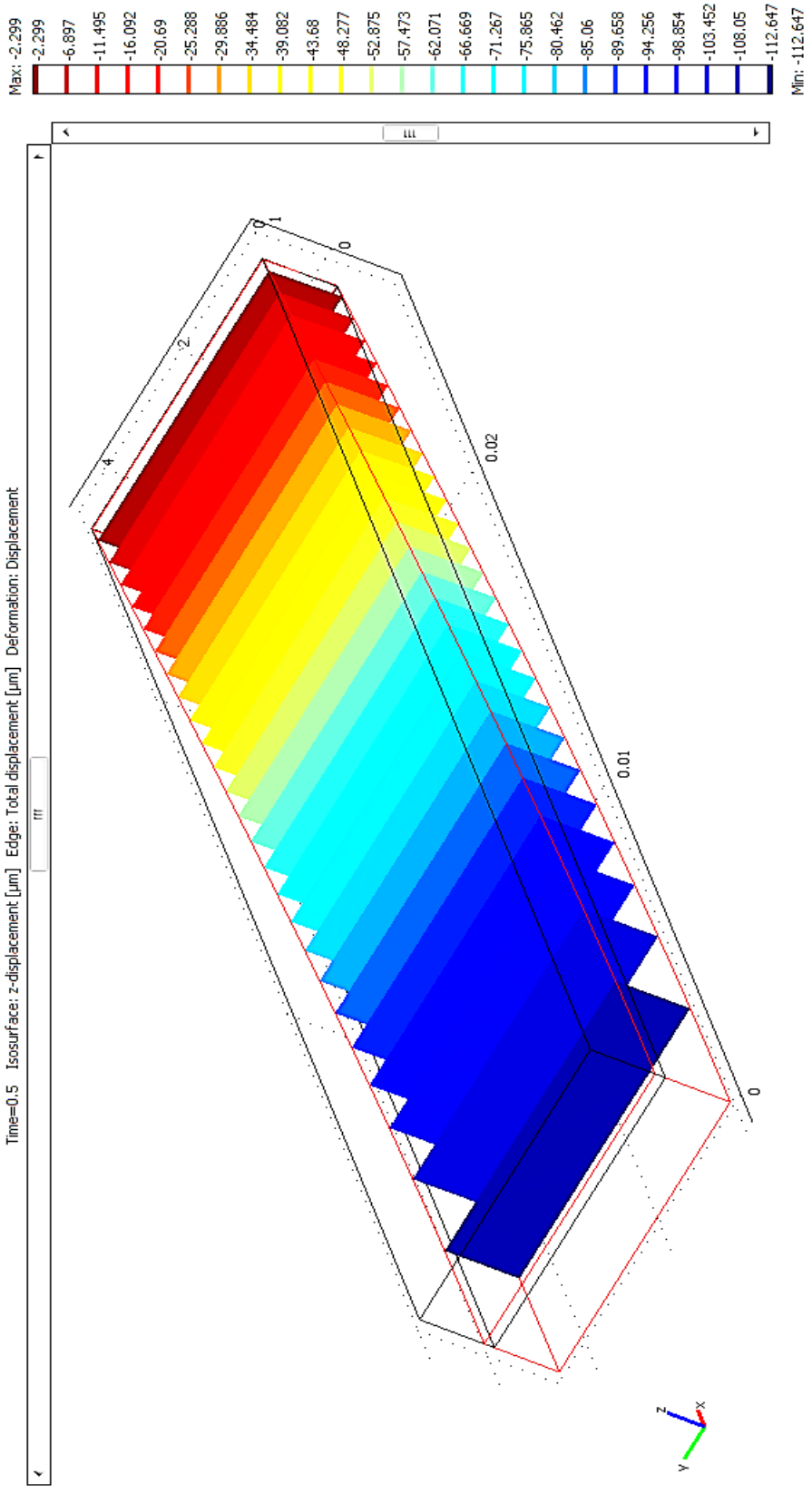

Figure 38: Maximum z-displacement (deformed shape outlined in red) of simulated plastic strip is about 112 µm: this value includes also the pre-bending displacement equal to 10 µm.

Manually introducing in the model the estimated value of this force, or deriving it by performing a static simulation for each material and geometry, permits to obtain results close to the experimental ones. However, a difference in pre-bending displacement of ± 1 µm, provokes the same variation in the calculated displacement of the sample at a given time. For instance, the difference of about 4% ("Δa" in Table 10) occurring between the corrected calculated and recorded displacements of the plastic specimen can be attributed to the action of the pre-bending force: in simulations it is always assumed that this force provokes a fixed displacement of 10 µm, while during the experimental measurements this value varied in the range 8–12 µm. For each geometry, the corresponding values of the Young's modulus are calculated from the corrected values of the displacement.

Following pictures show some results for the other two cases (aluminium and composite), attesting the origin of the values inserted in Table 10 and in Table 11.

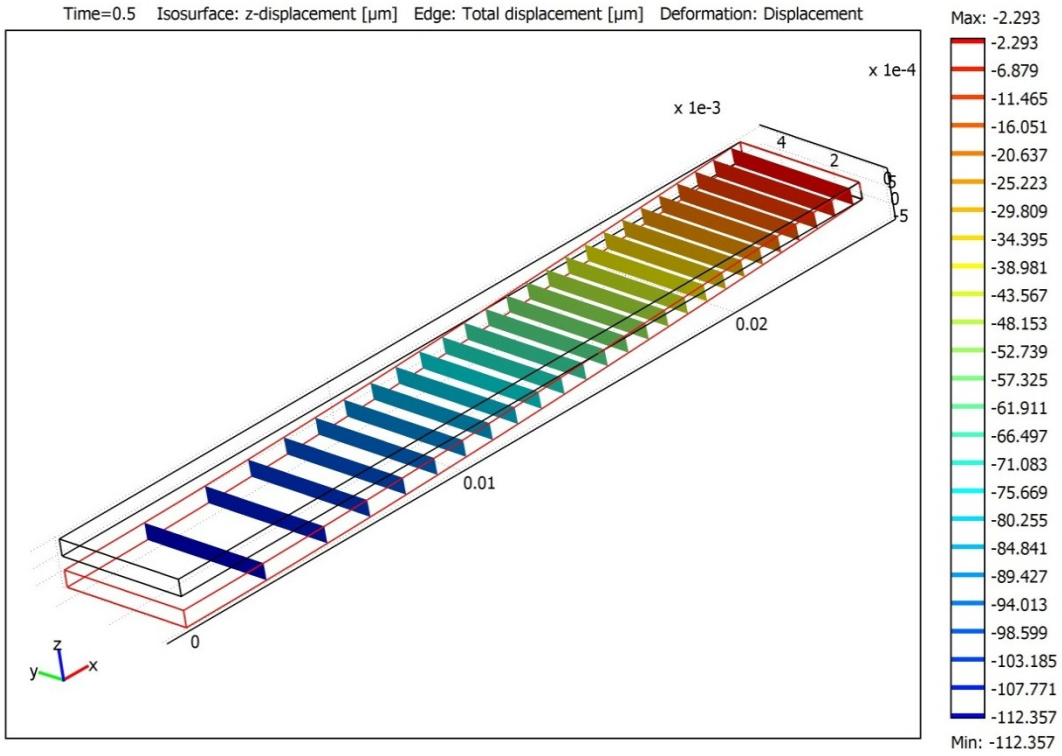

Figure 39: Z-displacement of the simulated aluminium specimen.

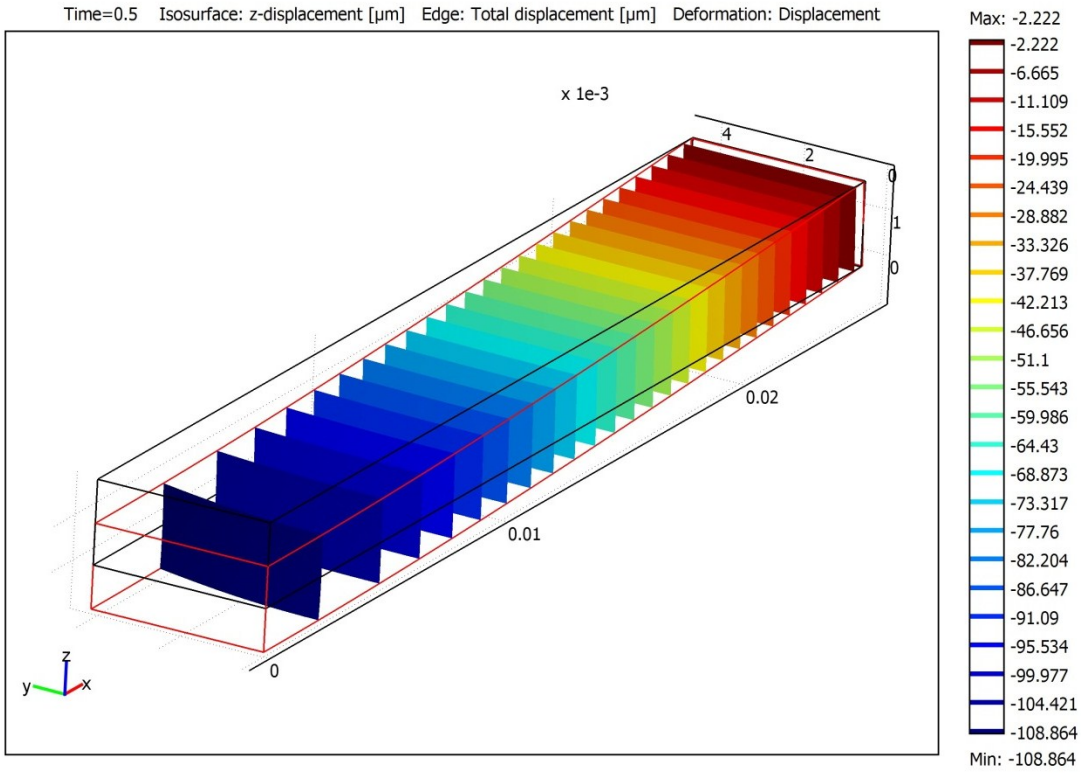

Figure 40: Z-displacement of the simulated composite (aluminium + plastic) specimen [µm]

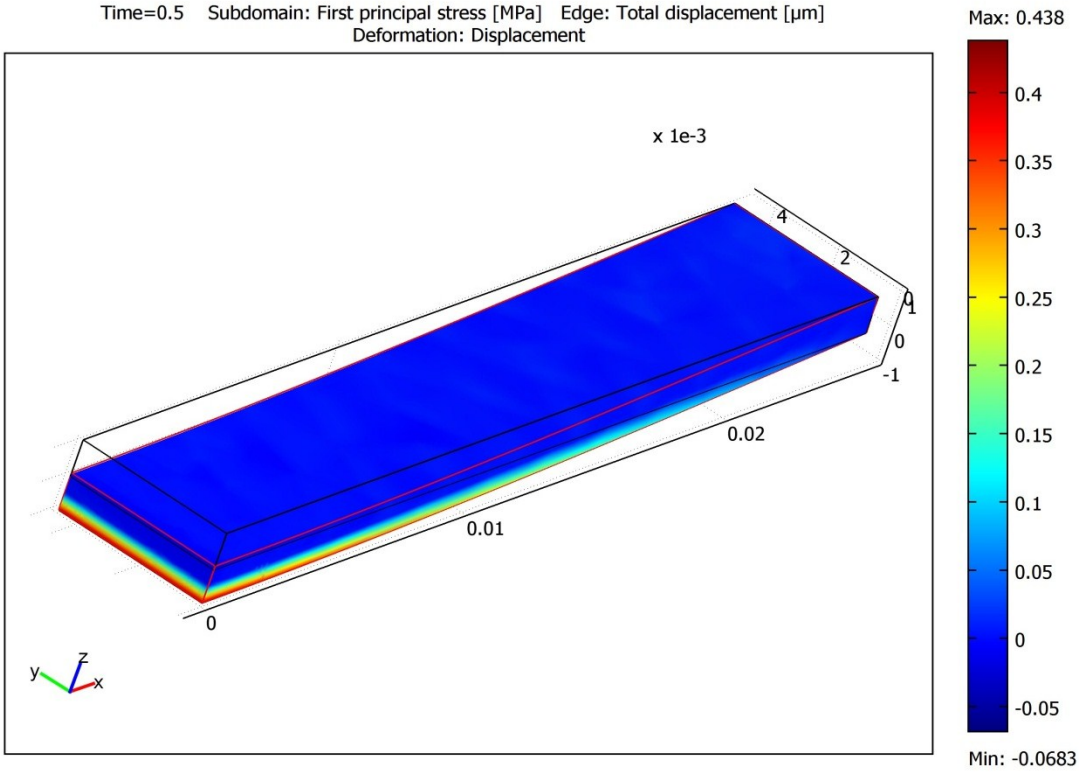

Figure 41: First principal stress [MPa] in plastic specimen, showing the tensile stress of 0.4 MPa in the lower face.

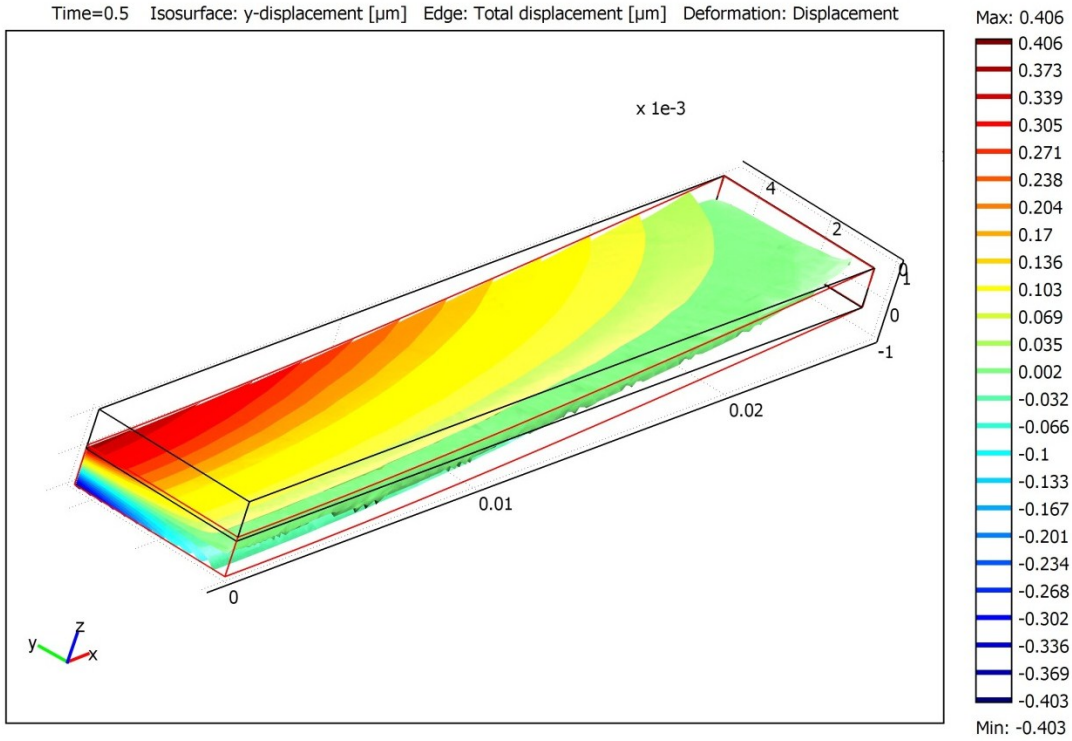

Figure 42: Displacement of the plastic specimen along the y-axis [µm]: effect of the Poisson's ratio is evident (compare with Figure 35).

The values presented in tables 10-11 confirm the reasonable goodness of the simulated results in their correlation with the DMA experimental data. The maximum error is less than 2% between measured and simulated Young's modulus values. This error can be also caused by unavoidable variations in specimens geometry: as expected from equation (6.3), small dimensional inaccuracies in thickness led to significant errors in output results (proportional to power of three). To eliminate this source of error, specimens with more precise dimensional tolerances should be used to improve the correlation between simulated and experimental results.

8 CONCLUSIONS

This work focused on the study of the behaviour of Ti-alloys for biomedical devices. Analysis of biomaterials requirements in their design was carried out, focusing on biomaterials for orthopaedic applications. In this field, metallic materials are the most used, due to their favourable mechanical and chemical properties, and titanium appears to be the first choice as prosthetic implant material. For understanding the problems in the bone replacement field, bone mechanical properties are examined, introducing the main factors involved in the challenge of making devices with a loading response as similar as possible to that of a real *living* bone.

Ti-alloys production and processing were also inspected, focusing on the relation between composition, thermo-mechanical treatments and final requested properties. The body-implant interaction is the more important aspect to take care during prosthesis design, as the bone and the implant act as a special composite material, which has to perform certain tasks without run into a premature failure. Based on these evaluations, Ti-alloys response to dynamic mechanical behaviour was simulated by FE analysis, and results from experimental measures were compared with those from the simulations.

Main results achieved during this final project can be summarized as follows:

- Between all metallic materials, cp-titanium and Ti-alloys resulted the best materials for orthopaedic applications, considering their high values of specific strength and corrosion resistance.
- The predominant position achieved by Ti-alloys is also remarked by their ability to allow osseointegration and by their low value of elastic modulus, which is closer to that of bone than any other implant material.
- Special solutions can be obtained with particular thermo-mechanical treatments of Ti-alloys, such as the so called “modulus adjusting”.
- A model capable to simulate the mechanical behaviour of Ti-alloys specimens undergoing three-point bending tests was built in COMSOL Multiphysics.
- Influence of different coating thickness and porosity on mechanical properties of Ti-alloys simulated specimens is analysed.

- Simulations showed that 0.7 mm thick Ti specimens are the best candidate to be coated and tested, meeting the requirements imposed by the available lab equipment.
- A linear variation of the coated specimens Young's modulus values is observed in simulations results, as well as the literature reports.
- Good correlation is achieved between calculated and experimentally tested values of displacement and corresponding Young's modulus values.

Some suggestions for further studies are proposed below:

- Real titanium specimens should be tested with the lab equipment to verify once more the results from the simulations.
- Future works should rely on the study of the material response with the presence of surrounding liquid, in order to take into account the poroelastic behaviour described in the literature part.
- Porous coated titanium specimens with different characteristics of coating thickness and porosity need to be tested, so that results can be compared with those from COMSOL simulations.

9 REFERENCES

[1] Allan et al, Biomaterials Science – An introduction to material in medicine, 3rd edition, Elsevier, 2013.

[2] E. Fjær et al., Petroleum related rock mechanics, 2nd edition, Elsevier, Oxford UK, 2008; pp. 1–43.

[3] S.T. Tsai, Composites Design, 4TH ed., Ohio 1988.

[4] http://en.wikipedia.org/wiki/File:Stress_Strain_Ductile_Material.png.

[5] H.P. Menard, Dynamic Mechanical Analysis, CRC Press, Taylor & Francis Group, Florida 2008; pp. 1–5, 71–93.

[6] M. A. Biot, General Theory of three-dimensional consolidation, J. App. Phys., 12, 1941, pp 155–164.

[7] K. Terzaghi, Erdbaumechanik, Franz Deuticke, Vienna, 1925.

[8] J. R. Rice, Elasticity of fluid infiltrated Porous solids, Harvard University Press, 1998.

[9] F.J. Valdes-Parada, Validity of the permeability Carman-Kozeny equation: a volume averaging approach, Physica A 388, 2009, pp. 789–798.

[10] E. Detournay and H.D. Cheng, Fundamentals of poroelasticity, in "Comprehensive Rock Engineering: Principles, Practice and Projects, Vol. II", Pergamon Press, 1993, pp. 113-171.

[11] COMSOL Multiphysics User's Guide, Version 3.5a, Earth Science Module, 2008.

[12] J. Y. Wong and J. D. Bronzino, Biomaterials, CRC Press, Taylor & Francis Group, 2007.

[13] J. B. Park, Biomaterials Science and Engineering, Plenum Press, New York, 1984.

[14] J. Black, The education of the biomaterialist: Report of a survey, Journal of Biomedical Materials Research 16, 1982, pp. 159-167.

[15] D.F. Williams, Definitions in biomaterials. Proceedings of a consensus conference of the European society for biomaterials, Elsevier, New York, 1987.

[16] J. A. Helsen and H. J. Breme, Metals as biomaterials, John Wiley and Sons, 1999, 1–72, 153–176.

[17] D.V. Rosato, in M. Szycher (Ed) Biocompatible Polymers, Metals and Composites, Technomic Publ, Lancaster, 1983, pp. 1019–1067.

[18] M. Kikuchi et al, The biomimetic synthesis and biocompatibility of self-organized hydroxyapatite/collagen composites, Bioceramics 12, 1999, pp. 393-396.

[19] J. Black, Biological performance of Materials: fundamentals of biocompatibility, CRC Press, Taylor & Francis Group ,New York, 2002.

[20] K. S.Katti, Biomaterials in total joint replacement, Biointerfaces 39, 2004, pp 133–14.

[21] J.D. Bronzino and D.R. Peterson, Biomechanics, principles and applications, CRC press, Taylor & Francis Group, 2008.

[22] M. Nordin and V.H. Frankel, Basic biomechanics of the musculoskeletal system, 4TH edition, Limppincott Williams & Wilkins, Baltimore, 2012, pp. 1–54.

[23] J. Currey, Bone Structure and Mechanics, Princeton University Press, 2002.

[24] J.L Katz et al., The effect of remodelling on the elastic properties of bone, Calcified Tissue International, 1984, 36 S31-S36.

[25] D.T. Reilly and A.H. Burstein, The mechanical properties of cortical bone, J Bone Joint Surg 56, 1974, pp. 1001–1022.

[26] M.F. Ashby, Material selection in Mechanical Design, Oxford, 2010.

[27] D.T. Reilly and A.H. Burstein, The elastic and ultimate properties of compact bone tissue; J.Biomech 8, 1975, pp. 393–405.

[28] H.S. Yoon and J.L. Katz, Ultrasonic wave propagation in human cortical bone; Measurements of elastic properties and microhardness, J Biomech 9, 1976, pp. 459-464.

[29] J. Wolff, Das Gesetz der Transformation der nochen, Berlin, 1892. The law of bone remodelling, translation by Maquel P and Furlong R, Berlin, Springer 1986.

[30] L.E. Lanyon et al; Bone deformation recorded in vivo from strain gauges attached to the human tibial shaft, Acta Orthop Scand 46, 1975, pp. 256–268.

[31] J. Currey, The mechanical adaptation of bones; Princeton University Press, 1984.

[32] A.H. Burstein et al, Bone strength: the effect of screw holes, J Bone Joint Surg 54, 1972, pp. 1143– 1156.

[33] W. Bonfield and P.K. Datta, Fracture toughness of compact bone, J Biomech 9, 1976, pp. 131–134.

[34] Garner et al, Viscoelastic dissipation in compact bone: implications for stress induced fluid flow in bone. J Biomech Eng 122, 2000, pp. 166-172.

[35] R. S. Lakes, Properties of bone and teeth, Encyclopedia of Medical Devices and Instrumentation, ed. J.G. Webster, J. Wiley, NY, 1988, pp. 523–536.

[36] G. Lütjering et al., Microstructure and mechanical properties of titanium alloys, Springer Verlag, pp- 1–47, 70–73.

[37] I.J. Polmear, Light alloys, from traditional alloys to nanocrystals, 4^{TH} edition, Elsevier 2006, pp. 363–365.

[38] A. Stwertka, Titanium, in "Guide to elements", Oxford University Press, 1998, pp. 81–82.

[39] G. Z. Chen, Forming Metal powders by electrolysis, in "Advances in powder metallurgy", Woodhead Publishing, UK, 2013, pp. 19–41.

[40] M.A. Imam et al., Titanium alloys in surgical implants, in "ASTM special technical application" 796, Philadelphia, 1983.

[41] Nakai and Niinomi, Recent progress in mechanically biocompatible titanium-based materials, in "Technological advancements in biomedicine for healthcare applications", IGI global, 2013, pp. 206–210.

[42] Nakai et al, Self-adjustment of Young's modulus in biomedical titanium alloys during orthopaedic operation, Materials Letters, 65, 2011 pp. 688-690.

[43] http://www.netzsch-thermal-analysis.com/en/products-solutions/dynamic-mechanical-thermal-analysis/dma-242-e-artemis.html.